Geochemistry Geophysics Geosystems G3
AN ELECTRONIC JOURNAL OF THE EARTH SCIENCES
Published by AGU and the Geochemical Society

Article
Volume 4, Number 5
9 May 2003
8607, doi:10.1029/2001GC000258
ISSN: 1525-2027

Stress-driven melt segregation in partially molten rocks

B. K. Holtzman, N. J. Groebner, and M. E. Zimmerman
Department of Geology and Geophysics, University of Minnesota, 310 Pillsbury Drive S.E., Minneapolis, Minnesota 55455, USA (holtz007@umn.edu; groe0029@umn.edu; zimme030@umn.edu)

S. B. Ginsberg
Department of Materials Science, University of Minnesota, Minneapolis, Minnesota, USA (ginsberg@aps.org)

D. L. Kohlstedt
Department of Geology and Geophysics, University of Minnesota, 310 Pillsbury Drive S.E., Minneapolis, Minnesota 55455, USA (dlkohl@umn.edu)

Department of Materials Science, University of Minnesota, Minneapolis, Minnesota, USA

[1] We demonstrate that deformation of partially molten ductile rocks can produce melt segregation by two-phase flow. In simple shear experiments on several melt-rock systems at high temperature and pressure, melt segregates into distinct melt-rich layers oriented 20° to the shear plane. Melt segregates in samples in which pressure gradients can develop at length scales less than the sample thickness. A simple scaling argument combined with a comparison of length scale data suggests that such pressure gradients can develop in the samples with compaction lengths less than or on the order of the sample thickness. In nature, stress-driven melt segregation may produce both high-permeability pathways that contribute to rapid extraction of melt and localization of deformation that increases the anisotropy in viscosity of partially molten regions of the upper mantle and lower crust.

Components: 13,230 words, 12 figures, 2 tables.

Keywords: melt segregation; deformation partially molten rocks; channel formation; mantle transport properties; mantle rheology; mantle seismic properties.

Index Terms: 3035 Marine Geology and Geophysics: Midocean ridge processes; 3902 Mineral Physics: Creep and deformation; 5112 Physical Properties of Rocks: Microstructure; 5114 Physical Properties of Rocks: Permeability and porosity; 5139 Physical Properties of Rocks: Transport properties.

Received 18 October 2001; **Revised** 22 October 2002; **Accepted** 1 November 2002; **Published** 9 May 2003.

Holtzman, B. K., N. J. Groebner, M. E. Zimmerman, S. B. Ginsberg, and D. L. Kohlstedt, Stress-driven melt segregation in partially molten rocks, *Geochem. Geophys. Geosyst.*, 4(5), 8607, doi:10.1029/2001GC000258, 2003.

Theme: The Oman Ophiolite and Mid-Ocean Ridge Processes
Guest Editors: Peter Keleman, Chris Macleaod, and Susumu Umino

1. Introduction

[2] In the Earth, stress enhances the migration of fluids by increasing the driving force for fluid movement and modifying the permeability structure of the matrix. This coupling between stress and melt migration has a substantial but poorly understood impact on the dynamics of mid-ocean

ridges, subduction zones, rising plumes, and lower crustal shear zones. At active mid-ocean ridges and in ophiolites, the observed chemical disequilibrium between the melt chemistry and the uppermost mantle peridotites requires that melt flows in localized high-flux conduits, chemically isolated from the surrounding mantle [e.g., *Spiegelman and Kenyon*, 1992]. For melt to be transported in channels from the mid-ocean ridge basalt (MORB) source region to the surface, small amounts of melt must first segregate from the partially molten rock. Melt transport to the surface then occurs by mechanisms ranging from channelized percolation through permeable viscous rock [e.g., *Kelemen et al.*, 1997] to flow through discrete open channels or fractures [e.g., *Nicolas*, 1986; *Rubin*, 1998; *Richardson et al.*, 1996; *Suhr*, 1999]. Any form of channelized flow is "self-organized" in the sense that the geometry of the channels is determined by the dynamics of the channel-forming process, not by any pattern inherent in the host rock. One well-studied mechanism for melt segregation and self-organization of channels is the reaction-infiltration instability [*Aharonov et al.*, 1995]. Here, we present new experimental evidence for the production of localized high-permeability channels in which the melt segregation and organization are driven by stress alone.

[3] In surface exposures of lower crustal and upper mantle rocks, interactions of deformation, melting, and melt segregation may be observed. Partially molten ductile rocks such as migmatites record interactions of strain localization and melt concentration in melt-rich shear zones [*Hollister and Crawford*, 1986; *Burg*, 1991; *Brown and Solar*, 1998], but the processes that produced the observed patterns are often obscured by overprinting. In the uppermost mantle exposed in ophiolites, the characteristic lack of obvious strain markers in the highest-temperature "asthenospheric" environments makes the interaction of melt migration and deformation less obvious. Tabular dunites, veins, and dikes observed in ophiolites are direct evidence for channelized melt flow, but the mechanisms of melt-segregation, channel-formation, and melt transport mechanisms are difficult to infer, as are the interactions of these processes with solid flow fields.

[4] These two phenomena, melt migration and solid deformation, have been considered together in models developed for the whole-ridge system [e.g., *Rabinowicz et al.*, 1987; *Phipps Morgan*, 1987; *Buck and Su*, 1989; *Spiegelman and McKenzie*, 1987; *Scott and Stevenson*, 1989; *Cordery and Phipps Morgan*, 1992]. Of these, the models which include the weakening effect of melt, either by imposing viscosity variations or self-consistently calculating a melt-fraction dependent viscosity, show that the weakening causes significant localization in the upwelling solid and fluid flow fields [e.g., *Rabinowicz et al.*, 1987; *Buck and Su*, 1989; *Scott and Stevenson*, 1989]. Further pursuit of these ideas has been limited by the difficulty in testing and constraining the models. An important constraint is to understand the mesoscale processes by which the melt weakens the solid and affects its flow (i.e., strain partitioning). The microscale processes of melt weakening are fairly well understood [e.g., *Hirth and Kohlstedt*, 1995a, 1995b]. However, upward scaling to anything other than a homogenous mantle is a difficult problem, partly because of the necessarily small scale of experimental samples and the difficulty of finding evidence for the mesoscale processes in the field. A few theoretical models have demonstrated that deviatoric stress can drive mesoscale melt segregation in pure water [e.g., *Stevenson*, 1989; *Richardson*, 1998; *Hall and Parmentier*, 2000]. However, these studies did not address the interaction of melt segregation and strain partitioning in the weaker melt-rich zones; the only interactions between the melt and solid flow fields were due to compaction, not shear. Thus, these studies do not provide a link between melt segregation, strain partitioning, and the large-scale flow of solid.

[5] Several field studies have demonstrated interactions of melt segregation and strain partitioning. Strain localization observed in dunites in the Josephine peridotite is evidence of the interaction of deformation and melt migration produced under lower temperature conditions (1223-1373 K) [*Kelemen and Dick*, 1995]. Recently, *Dijkstra et al.* [2002] have demonstrated that melt weakening may play an important role in influencing flow in the uppermost mantle preserved in the Hilti massif, Oman ophiolite, following studies by *Ildefonse et al.* [1995] and

Michibayashi et al. [2000]. However, in all four of these studies, the outcrop evidence of these processes lies in locations in ophiolites inferred to be "off-axis". In other words, processes that left traces during upwelling have been overprinted by subsolidus mantle flow through the corner beneath the spreading center, and processes that occurred after the mantle flow rotated toward the horizontal experienced different conditions than in the upwelling flow. However, more direct inferences of melt-migration/strain localization processes during upwelling may be possible in locations believed to represent near-axis conditions, as done by *Ceuleneer and Rabinowicz* [1992], discussed in section 5.6.2.

[6] The experiments described in this paper demonstrate that deformation and melt segregation are inextricable processes during flow of partially molten rocks. Our experimental results offer a simple means to scale these processes upward to the meso- and macroscales of mantle flow. Recent experimental studies of samples deformed in the ductile regime confirmed that stress changes melt topology and thus strongly influences the mechanics of melt migration. Samples of olivine + MORB deformed to large strains in simple shear develop a pronounced melt preferred orientation defined by interconnected grain-scale melt pockets subparallel to the applied stress [*Zimmerman et al.*, 1999]. Melt segregation features were also reported in two other experimental studies of deforming partially molten materials in shear. In sheared samples of fine-grained quartzite, *Dell'Angelo and Tullis* [1988] found very small amounts of a melt phase in pockets aligned in a similar orientation to that found in the olivine + MORB samples, spaced several grain diameters apart. In shear deformation experiments on norcamphor with a benzamide melt, the melt migrated from uniformly distributed melt pockets into shear zones as shear strain increased and melting continued [*Rosenberg and Handy*, 2000]. These segregations have some similarities with ours, but may represent more brittle phenomena, due to the lack of confining pressure and to the increase in melt pressure due to in situ melting. In this paper, we show that melt can further redistribute, or segregate, into oriented melt-rich layers over scales larger than the grain scale. We are able to predict the conditions under which melt segregation occurs in experiments and explain the morphologies of the melt-rich bands using a simple scaling argument involving the "compaction length", defined below. This approach suggests a method for further mechanical analysis of the experiments and a potential means of scaling from laboratory to geologic conditions.

2. Compaction Length and Melt Segregation

[7] Two-phase compaction theory describes the behavior of a melt phase migrating through a deforming partially molten rock [e.g., *McKenzie*, 1984; *Scott and Stevenson*, 1986; *Bercovici et al.*, 2001a]. The resulting equations are nondimensionalized using a characteristic length scale called the compaction length, δ_c. The compaction length of a partially molten sample is determined by the permeability, k, the melt viscosity, μ, the bulk viscosity, λ, and the shear viscosity, η, of the partially molten rock as expressed by the relation [*McKenzie*, 1984; *Scott and Stevenson*, 1986]

$$\delta_c = [k[\lambda + (4/3)\eta]/\mu]^{1/2}. \quad (1)$$

We use the simplified form $\delta_c = [k(4/3)\eta]/\mu]^{1/2}$ [*Daines and Kohlstedt*, 1993], assuming that $\lambda \ll \eta$ [*Richardson*, 1998; *McKenzie and Holness*, 2000]. To extrapolate viscosity to higher and lower melt fractions, an expression of the form

$$\eta = \eta_0 \exp(-\alpha\phi), \quad (2)$$

was suggested by *Kelemen et al.* [1997], with α = 45, based on a compilation of published experimental creep data, and where η_0, the pre-exponential factor, is a function of temperature and pressure (see section 5.4). We use a more recent estimate of α = 25 determined for olivine + MORB [*Mei et al.*, 2002].

[8] Permeability is calculated using the relation, described in Appendix A,

$$k = \phi^n d^2/b \quad (3)$$

with n = 2 or 3 when channels approximate tubes or sheets, respectively, d is the grain diameter, and b is a geometric factor, with values given in Table 1

Table 1. Summary of Experimental Parameters and Calculated Values of Compaction Length for the Partially Molten Systems Explored in This Study[a]

Sample	ϕ	d, m	b	k, m^2	η, Pa.s	μ, Pa.s	δ_c, m	δ_c/δ_t	Bands?
olv. + MORB	0.03	2×10^{-5}	1×10^{3}	3.6×10^{-16}	2.2×10^{12}	10	1.0×10^{-2}	10.5	no
an. + MORB	0.03	4×10^{-6}	1×10^{3}	1×10^{-17}	5.9×10^{11}	10	1.0×10^{-3}	1.4	yes
olv. + chr. + MORB	0.02	1×10^{-5}	1×10^{4}	5×10^{-18}	6.2×10^{11}	10	5.7×10^{-4}	0.8	yes
olv. + chr. + MORB	0.06	1×10^{-5}	1×10^{4}	5×10^{-17}	4.2×10^{11}	10	1.4×10^{-3}	2.1	yes
olv. + chr. + MORB	0.12	1×10^{-5}	1×10^{4}	1×10^{-16}	1.6×10^{11}	10	1.6×10^{-3}	0.2	yes
olv. + alb. − melt	0.03	7×10^{-6}	1×10^{3}	4×10^{-17}	5.5×10^{12}	3.3×10^{5}	3.1×10^{-5}	0.05	yes

[a] Values of k were calculated from ϕ, d, and b; values of η were calculated for all samples from strain rates measured at a shear stress of 50 MPa; values of μ were determined from quantities reported in the literature. Values of δ_c were calcuated with equation (4). Note that if the ratio $\delta_c/\delta_t \lesssim 1$, melt tends to segregate into bands during deformation.

[*Turcotte and Schubert*, 1982]. Equations (1)–(3) are combined to give the expression for compaction length used throughout the paper:

$$\delta_c = \left[\left(\phi^n d^2/b\right)(4/3)\eta_0 \exp(-\alpha\phi)/\mu\right]^{1/2} \quad (4)$$

[9] In gravity-driven melt extraction, this length scale is the vertical distance "over which the compaction rate decreases by a factor of e" [*McKenzie*, 1984]. δ_c may also be thought of as the distance over which melt flow and matrix deformation are coupled. In a gravity-driven system, the matrix deforms in response to melt extraction, since no pore space can open. In a stress-driven problem, like the one at hand, stress applied to the partially molten rock creates the pressure differences that drive melt migration, as shown by *Cooper* [1990].

[10] In this study, δ_c is used as a physical property of a partially molten system. In a system with a homogeneous melt distribution, δ_c will be an average property; when melt begins to segregate, δ_c quickly becomes spatially varying. We calculate the initial compaction length for each system used in this study. The guiding notion is that the ratio δ_c/δ_t determines if stress can drive melt segregation, where δ_t is the thickness of the sample. Varying this ratio is a similar approach to that used by *Renner et al.* [2003] for drained triaxial compaction experiments. If $\delta_c/\delta_t \gg 1$, pressure gradients will not develop in the fluid because the fluid moves too easily through the system (either because of high permeability or low melt viscosity) and can quickly relax any fluid pressure gradients. If $\delta_c/\delta_t \lesssim 1$, then the system is much more sensitive to small perturbations in melt fraction (because the composite viscosity depends strongly on melt fraction), and fluid pressure gradients can develop leading to melt segregation. The stress fields then determine the orientation of segregated regions. These notions are tested by varying the initial compaction lengths of several partially molten systems.

3. Experimental Design

3.1. Varying δ_c

[11] We investigated stress-driven melt segregation in four types of partially molten rocks with different compaction lengths using simple shear experiments in a gas-medium deformation apparatus [*Zimmerman et al.*, 1999]. We calculated the initial (predeformation) compaction length for each sample using published values for μ, measured values for η, and estimated values for k. We determine viscosity from the ratio of equivalent stress to equivalent strain rate [*Poirier*, 1985, p. 10]. For non-Newtonian behavior, viscosity is a function of stress, so for the experiments deforming in dislocation creep (stress exponent n >3), the viscosity value is associated with a specific value of stress. For consistency, viscosities given in Tables 1 and 2 were calculated at a shear stress of 50 MPa (equivalent stress of 100 MPa), a stress achieved early in the deformation of most of the samples.

[12] Estimates of permeability for all samples were based on a value for olivine +10 vol% MORB obtained in the following manner: 1) A 3-D form of the melt-filled volume was created by serially sectioning a sample and interpolating the volume between the images. 2) Flow through this volume was simulated with a lattice-Boltzmann calculation, which provides an estimate of the permeabil-

Table 2. Experimental Conditions and Results[a]

Sample	ϕ,[b]	γ	T, C	P, MPa	$\dot{\gamma}$[c] @50 MPa	η @50MPa	σ, f	$\dot{\gamma}$, f	Bands?	Angle[d]	Spacing, δ_b[e]
						Olivine + MORB					
273	0.03	2.3	1250	300	8.10×10^{-5}	2.19×10^{12}	83	4.6×10^{-4}	no	–	–
356	0.03	2.6	1250	300	3.20×10^{-5}	1.56×10^{12}	122	1.4×10^{-4}	no	–	–
358	0.03	2	1250	300	6.30×10^{-5}	7.94×10^{11}	90	4.1×10^{-4}	no	–	–
628	0.10	2.5	1250	300	2.50×10^{-5}	2.00×10^{11}	90	1.7×10^{-3}	no	–	–
729	0.03	2	1250	300	6.30×10^{-5}	7.94×10^{11}	90	1.20×10^{-4}	no	–	–
						Anorthite + MORB					
763	0.05	3	1200	300	–	–	–	–	yes	–	–
776	0.05	3	1200	300	–	–	–	–	yes	–	–
779	0.05	3	1200	300	–	–	–	–	yes	–	–
786	0.05	3	1200	300	3.16×10^{-4}	5.89×10^{11}	55.3	3.3×10^{-4}	yes	15 ± 4	83 ± 28
						Olivine + Chromite + MORB					
884	0.02	1.1	1250	300	N.R.E.	–	68.1	2.2×10^{-4}	yes	17 ± 6	~20
889	0.02	2.1	1250	300	N.R.E.	–	82	2.7×10^{-4}	yes	22 ± 13	~50
833	0.02	3.3	1250	300	7.20×10^{-4}	6.17×10^{11}	87	4.2×10^{-3}	yes	22 ± 6	97 ± 32
885	0.06	1.1	1250	300	N.R.E.	–	64.9	6.7×10^{-4}	weak	–	–
891	0.06	2.1	1250	300	N.R.E.	–	68.4	1.5×10^{-3}	yes	17 ± 5	~50–100
830	0.06	3.5	1250	300	8.33×10^{-4}	4.17×10^{11}	75.1	9.8×10^{-4}	yes	17 ± 6	195 ± 94
902	0.06	3.5	1250	300	6.60×10^{-4}	7.58×10^{10}	64.9	3.7×10^{-3}	yes	16.4 ± 6.9	40 ± 20
825	0.12	3.5	1250	300	1.10×10^{-3}	1.55×10^{11}	51.6	4.1×10^{-3}	yes	~20	283 ± 128
						Olivine + Albitic Melt					
836	0.03	2.5	1250	300	2.51×10^{-5}	5.50×10^{12}	160.2	3.1×10^{-4}	weak	–	–
839	0.03	2.5	1250	300	N.R.E.	–	150.8	2.9×10^{-4}	weak	–	–
847	0.03	5.05	1250	300	N.R.E.	–	193.7	1.5×10^{-3}	yes	~20	17 ± 8
850	0.03	4.9	1250	300	N.R.E.	–	210	2.9×10^{-3}	yes	~20	16 ± 8

[a] Symbols: ϕ, melt fraction; γ, shear strain; $\dot{\gamma}$, shear strain rate; η, viscosity; σ, shear stress. An "approximate" sign (~) indicates an estimate without statistical measurement. N.R.E indicates that stress values were too high to extrapolate reasonably down to 50 MPa.
[b] Post hot press, predeformation melt fraction (±0.01). The total final melt fraction is very difficult to measure once the melt has segregated into bands.
[c] Shear stress, which is half the differential stress.
[d] Mean angle of band relative to shear plane in degrees.
[e] Average spacing between largest bands, measured by linear intercept method normal to bands.

ity, performed by Joanne Frederich, reported by *Scott* [2000], and described in more detail in Appendix A. We use this value for one sample to calculate the geometric parameter, b, in the permeability expression, equation (3), and use simple arguments described below and in Appendix A to estimate permeability in other systems relative to the quantitative value.

[13] In the rock samples described below, the values of k, μ and η are varied relative to those of olivine + MORB for which a large database already exists [*Kohlstedt and Zimmerman*, 1996]. The critical parameters for the partially molten systems investigated here are summarized in Table 1.

[14] 1. η: Anorthite + MORB samples have a lower viscosity than olivine + MORB samples because the viscosity of anorthite is lower than that of olivine at the temperatures of the experiments [*Dimanov et al.*, 1998; S. B. Ginsberg and D. L. Kohlstedt, personal communication, 2001]. The viscosities of the olivine + chromite + MORB samples are also lower than olivine + MORB because chromite grains inhibit growth of olivine grains, thus allowing a greater contribution to the deformation from diffusional grain-size sensitive creep processes [*Holtzman*, 2003].

[15] 2. k: a) Olivine + chromite + MORB samples have lower permeability than olivine + MORB samples because small chromite grains clog melt channels, increasing their tortuosity (see Appendix A). In addition, increasing the melt fraction systematically increases k, as described in equation (3), providing variation among the samples deformed. b) Because the melt distribution in

anorthite + MORB samples is similar to that in olivine + MORB samples, the same geometric factor b in the permeability expression was used in both cases. This assumption is based on relatively little quantitiative data. The anisotropic surface tension of anorthite-basalt system [e.g., *Lamoureux et al.*, 1999] causes the pocket shape to be more disk-like than in the olivine-MORB system, thus lowering the permeability normal to the disks relative to the olivine + MORB system. Our permeability estimate may therefore be high. c) Olivine + albitic melt samples appear to have the same permeability as the olivine + MORB samples, except for the difference in average grain size.

[16] Permeability is the greatest source of uncertainty in the calculated values of compaction length. Since all values of permeability are estimated relative to the value for olivine + MORB, we believe that the relative, if not the absolute, differences are meaningful. To account for the uncertainty in our calculations of compaction length, we place an error estimate of 25% on the values plotted in Figures 7 and 8.

[17] 3. μ: Olivine + albitic melt samples have a higher melt viscosity than olivine + MORB samples [*Urbain et al.*, 1982]. The viscosity of the melt in contact with olivine and anorthite was calculated with the thermodynamic phase equilibria program MELTS [*Ghiorso and Sack*, 1995], which determines melt viscosity using the formulation of *Shaw* [1972].

3.2. Experimental Details

[18] Our samples were deformed in a simple shear geometry in a gas-medium apparatus, as illustrated in Figure 1, at a confining pressure of 300 MPa and a temperature of 1523 K, except for the anorthite samples, which were deformed at 1473 K. Samples were placed between tungsten pistons cut at 45° to the compression axis. Grooves were cut into the pistons to improve gripping with the sample; their approximate form is that of a sine wave with an amplitude of 20 μm and a wavelength of 250 μm. To test the effects of the grooves on melt distribution and band formation, we performed one experiment using ungrooved pistons cut from single crystals of olivine, oriented with the easy-slip plane, (010), normal or parallel to the maximum principle stress. At high temperature, T, and pressure, P, the piston bonds to the sample interface by diffusively eliminating grain boundaries of similarly oriented grains.

[19] We deformed synthetic samples prepared from d $\approx$ 10 μm powders of crystals and d $\approx$ 1 μm powders of melt phases in the following combinations: 1) San Carlos olivine plus 2 or 5 vol% MORB. 2) Synthetic and natural anorthite plus 3 vol% MORB. 3) San Carlos olivine and Oman chromite mixed in a 3:1 volume ratio plus 2, 6 or 12 vol% MORB. (The chromite has a Cr/Cr + Al ratio of 0.5.) 4) San Carlos olivine plus 3 vol% albitic melt. The experimental conditions are described in more detail in Table 2. Sections of the deformed samples were cut perpendicular to the shear plane in the direction of maximum shear strain for analysis in reflected light and scanning electron microscopy (SEM). Samples were etched in a weak HCl/HF solution to improve visibility of melt pockets. Spacings between melt bands were measured with a linear intercept method in the following manner. At a low enough magnification of the etched samples in reflected light, the bands appear as discrete objects, as opposed to gradational wave-like variations in the concentration of melt pockets. We drew lines across the image normal to the band orientation (crossing steepest gradients in melt fraction), spaced at intervals large enough to minimize repetitive data, and the ends of the sample were avoided by a distance approximately equal to the sample thickness. The spacings between the largest bands were measured on each line. The definition of largest bands is somewhat subjective. In most cases, it was clear, because the large bands are few and very visible; any band less than about half the width of the largest band was considered to be secondary. The number of large bands in each sample is very small, but the differences between samples are clearly visible in the images and are reflected in the data.

4. Results

[20] A continuum of melt-distribution behavior results from deformation of samples from each

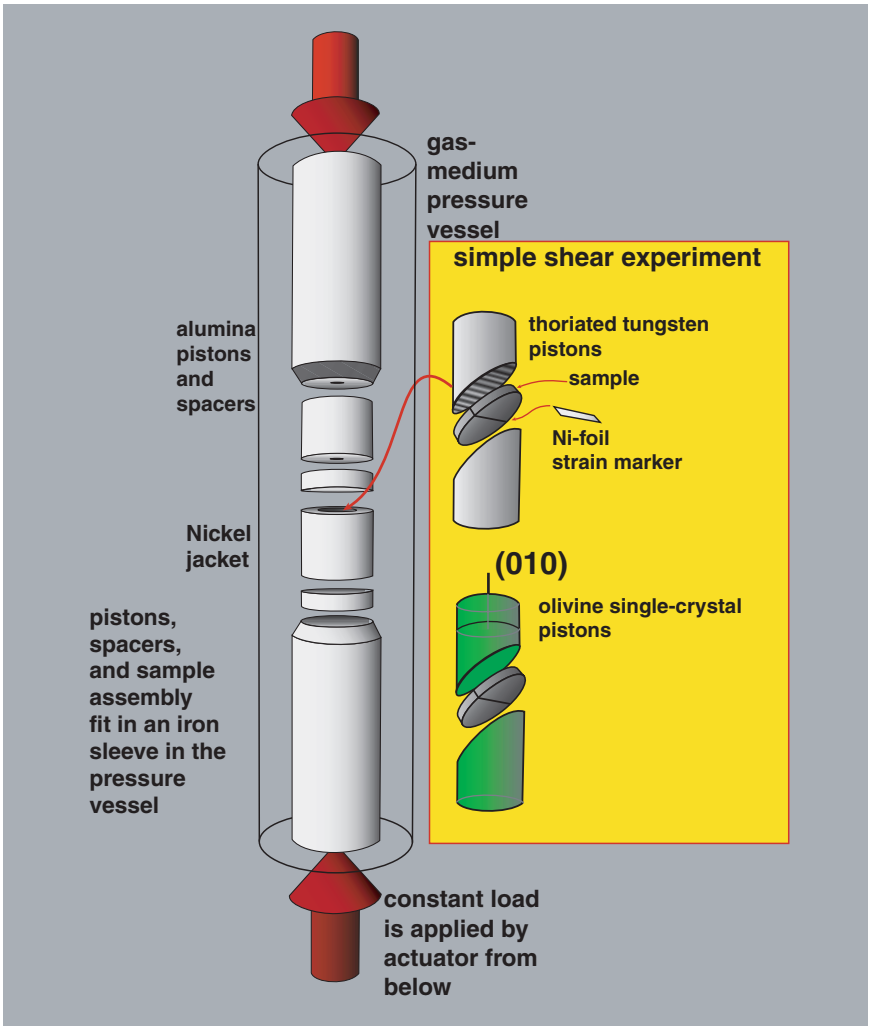

Figure 1. Experimental apparatus. The sample assembly fits into an Fe jacket, not shown. The transparent outer cylinder represents the inner wall of the furnace inside the pressure vessel. The central assembly is surrounded by Ar gas at 300 MPa, which convects around the sample, providing an even temperature profile. The sample is ~1 mm thick. The other parts of the assembly are pictured roughly to scale.

system. On one end of this continuum, shear deformation creates a marked anisotropy in melt distribution, as melt redistributes from randomly oriented melt-filled pockets into pockets with a strong preferred orientation, but segregation does not occur beyond the grain scale. On the other end, melt segregates strongly into melt-rich bands with thicknesses and spacings larger than the grain scale, but with the same orientation as the melt pockets. The subject of this paper is the longer wavelength segregations imposed on the grain-scale variations.

[21] In samples of olivine + MORB, only the melt pockets align, but longer wavelength segregations do not develop. In the other three systems, the longer wavelength melt bands are superimposed on the first-order melt pocket alignments. In all experiments in which bands form, the distribution of bands included fewer large bands and more numerous, more closely spaced smaller bands between them. In this paper, we only discuss the spacing between the larger bands; more detailed statistical studies of the band distribution will follow.

[22] In each system, samples were deformed to several different finite strains. Since the initial melt distribution is homogeneous over lengths longer than the grain scale, the melt distributions always progress through the continuum described above,

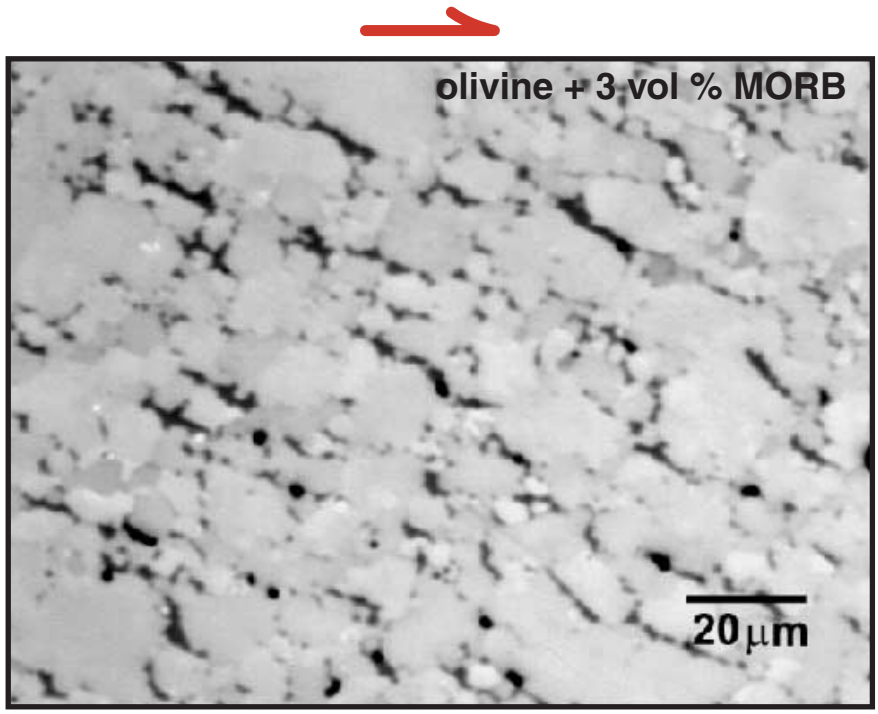

Figure 2. Reflected light optical micrograph of an olivine + MORB sample (PI-273). The melt pockets (dark) strongly align at about 20° to the shear plane (horizontal). The melt distribution is homogeneous across the sample. (Modified from *Kohlstedt and Zimmerman* [1996] and *Zimmerman et al.* [1999].)

such that the melt distribution is a function of time. We do not claim that any melt distribution reaches a steady state, though this question will be addressed in much greater detail in future papers. Therefore, when melt distributions between samples are compared, samples deformed to the same strain were selected, wherever possible. In Table 2, the experimental conditions and average properties of the melt fraction distributions are listed for each sample. In the following sections, the results from each group of experiments are described.

4.1. Olivine + MORB

[23] In sheared samples of olivine + 3 vol% MORB, melt is uniformly, but anisotropically, distributed across the sample in grain-scale pockets oriented 25° to the shear plane (20° from the maximum principal stress), as illustrated in Figure 2 (modified from *Kohlstedt and Zimmerman* [1996] and *Zimmerman et al.* [1999]). The melt pockets, spaced approximately a grain width apart, form parallel interconnected volumes often several grains long, which more closely approximate sheets than tubes in 3-D (see Appendix A). Sixteen samples were deformed, at varying stresses and to varying strains, none of which formed bands. Five of these samples are listed in Table 2.

4.2. Anorthite + Basaltic Melt

[24] During deformation, melt migrates into melt-rich bands ~20 μm wide and ~100 μm apart, as shown in Figure 3. The bands are oriented ~10–20° to the shear plane. The bands appear to form anastomosing networks. A high-resolution SEM image of a band reveals a very high melt fraction and euhedral grains, lying "piggyback" on each other, providing a clear sense-of-shear indicator, as illustrated in Figure 3b. In addition, many of these bands root from or feed into small regions of locally high melt fraction on the low-pressure side of the peaks in the tungsten pistons.

4.3. Olivine + Chromite + MORB

[25] Eight shear experiments are reported here on this system, with varying melt fractions and finite

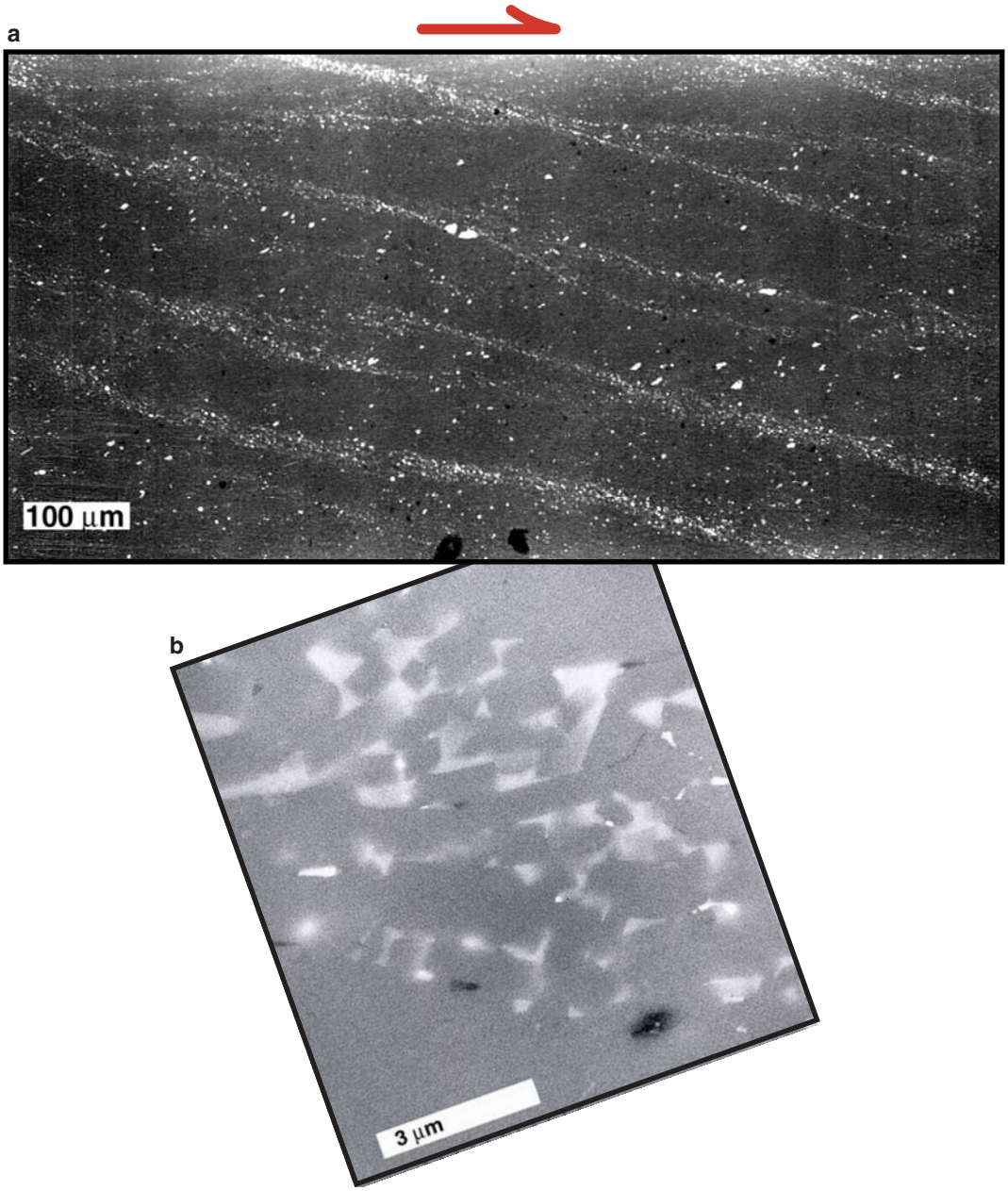

Figure 3. Scanning electron micrographs of anorthite + MORB samples deformed to g = 3. a) PI-786. In this SEM image, the melt-rich bands appear as whitish streaks. In some regions, every piston groove has an associated band but not every band a groove. b) PI-763. The gray phase is anorthite; the whitish material is composed of clinopyroxene and glass. Note the smaller-than-average euhedral grains with a shape fabric suggesting a top-to-the-right shear. The image is rotated so that the band is in its approximate orientation relative to a), though they are not from the same sample.

strains. Three samples with $\phi = 0.02$ and three with $\phi = 0.06$ were sheared to shear strains, γ, of 1, 2, and 3–3.5. One sample with $\phi = 0.12$ was deformed to a strain of 3.5. An additional sample with $\phi = 0.06$ was deformed with pistons made from olivine single crystals instead of tungsten. Micrographs of this sample, in Figure 4, illustrate that bands form without the presence of grooves on the piston walls. The following comparisons between samples are all made for those deformed

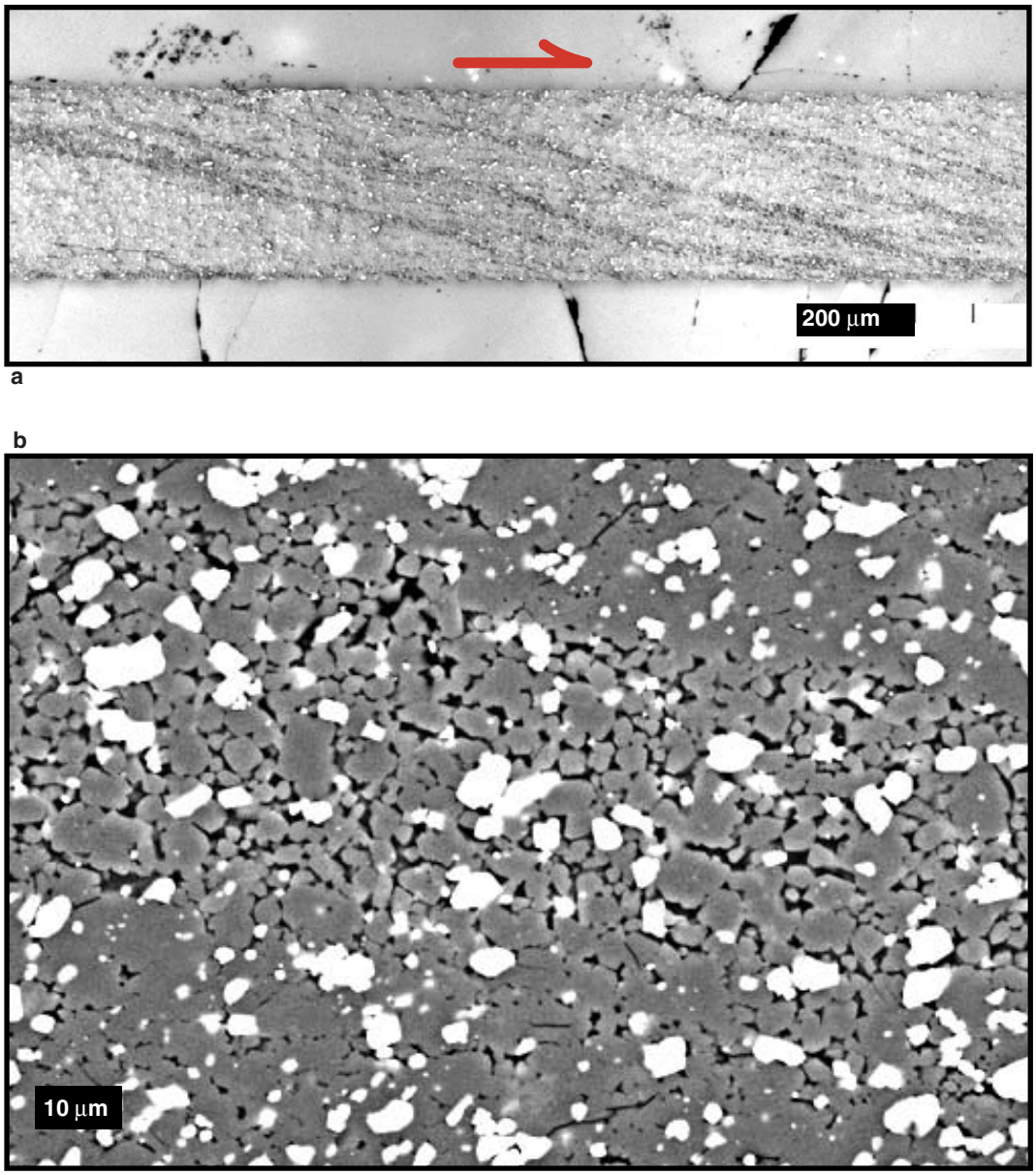

Figure 4. Micrographs of an olivine + chromite + 6 vol% MORB sample (PI-902) deformed to a shear strain of 3.5 between pistons made of olivine single crystals. a) In this reflected light image, the melt-rich bands appear as dark streaks oriented 20° to the shear plane (the piston wall). b) This SEM backscattered electron image of one typical band illustrates the dramatic segregation of melt. Chromite is white, olivine is gray, and melt is black.

with tungsten pistons. (The sample with olivine pistons is much thinner than the others, which may complicate direct comparison.)

[26] Bands form in the $\phi = 0.02$ series at a shear strain of 1 (PI-884), and in the $\phi = 0.06$ (PI-891) series by a strain of 2. With increasing strain, bands become wider and the spacing between them increases. We cannot establish whether these morphologies already have or will reach a steady state; we can only compare morphologies between different samples at similar finite strains. The evolution of melt segregation will be discussed in much greater detail in subsequent papers.

[27] At shear strains of 3–3.5, melt bands develop in samples with all three melt contents (0.02, 0.06 or 0.12, PI-833, PI-830, and PI-825, respectively),

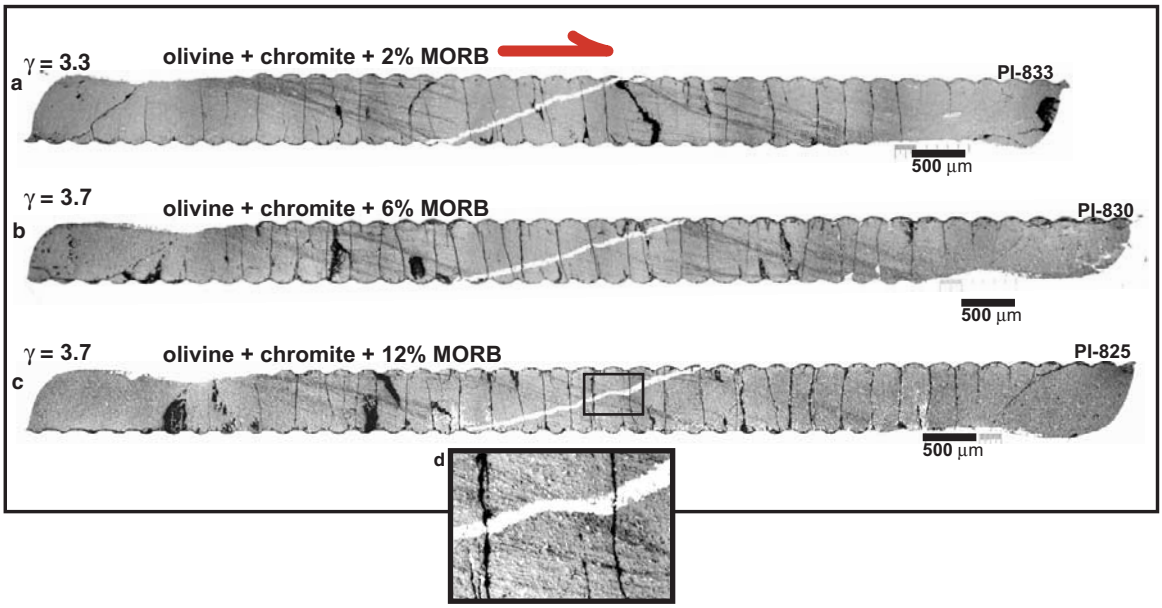

Figure 5. Reflected-light optical micrograph of olivine + chromite + 2, 6, and 12 vol% MORB samples (PI-833, PI-830, PI-825). These three samples were deformed to a shear strains of 3.3–3.7. In these reflected-light images of acid–etched samples, the bands appear as dark gray streaks 15–20° to the shear plane. The vertical dark lines are quench cracks, and should be ignored. The white lines are the nickel strain markers. Note in the 12% sample, where bands cross the strain marker, it is clearly offset, with a sense of shear similar to that observed in the anorthite + MORB samples. The bands increase in thickness and spacing with melt fraction, which is also an increase in compaction length.

oriented 15–25° to the shear plane, as shown in Figure 5. These angles are slightly higher than in the anorthite + MORB samples. In the three samples deformed to $\gamma = 3–3.5$, the width of and spacing between bands increases systematically with increasing melt fraction. In the sample with $\phi = 0.12$, only a small number of wide and diffuse bands developed; also, one small band cuts across and displaces the strain marker, also illustrated in Figure 5d. (Another indication that shear slip localized on the bands is described above in the anorthite + MORB sample (Figure 3b).) Often, bands have an asymmetric distribution of melt in which one border of a band is diffuse and the other is abrupt; the abrupt transition is often on the side of the band facing the oncoming simple shear flow of solid material.

4.4. Olivine + Albitic Melt

[28] Of four samples, two were deformed to shear strains of $\gamma = 2.5$ and two to $\gamma = 5$. In the samples sheared to $\gamma = 2.5$, melt is distributed in planar or disc-shaped, oriented, connected pockets that span the length of several grain diameters. The melt effectively forms sheets separated by at least one grain diameter, at 15–20° to the shear plane. The distribution of these bands normal to their lengths is not distinct; segregation at length scales larger than the grain scale is difficult to delineate. In the two samples sheared to higher strains, melt segregation is apparent, but the spacings between bands are smaller than in both the anorthite and olivine + chromite samples, as illustrated in Figure 6. The morphology of bands is more irregular than in the other systems; the bands are sometimes very sharp and narrow, almost like very long melt pockets, and elsewhere very diffuse undulations in melt fraction. A single band may widen and narrow along its length. Local, but not average, grain growth appears to have been rapid in these samples, which, together with the highly viscous melt (and associated lower olivine diffusivity through melt) resulted in the high strength of these rocks relative to the olivine + MORB samples. However, the smaller average grain size of the olivine +

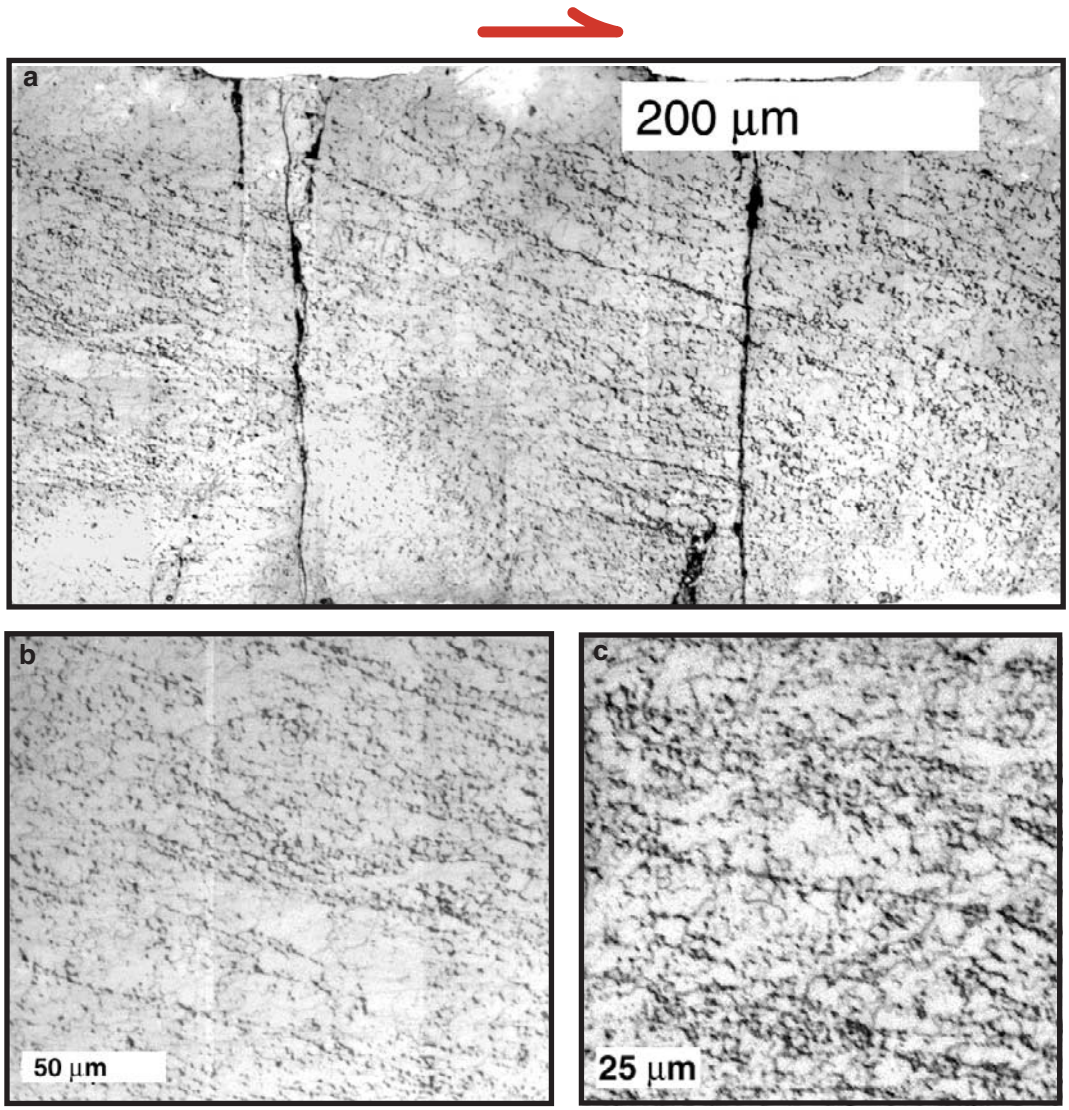

Figure 6. Reflected light micrographs of olivine + albite melt samples (PI-847 (a,b) and PI-850 (c)). These samples, which were deformed to $\gamma = 5$, developed narrow and closely spaced melt bands (dark). The morphology of these bands is quite different than the other systems. They pinch and swell along their lengths, from bands several grains wide to bands that seem to be one continuous melt pocket stretching the length of many grains. These long pocket-wide bands are different from the oriented pockets observed in the olivine + MORB system; they are much longer and are continuous with wider, more diffuse sections of the same band.

albitic melt samples causes their permeability to be lower than that of the olivine + MORB samples.

5. Discussion

5.1. Compaction Length and Band Formation

[29] Comparison of the observed melt distributions (the absence or presence of bands) with the calculated compaction lengths leads to two conclusions:

[30] First, melt segregation occurs if the compaction length and the sample thickness are similar, or more specifically, if $\delta_c/\delta_t \lesssim 1$. Segregation does not occur when $\delta_c/\delta_t \gg 1$, as in the olivine + MORB samples. This point is illustrated in the plot of δ_c against ϕ, in Figure 7. The compaction lengths of the band-forming systems are very close to the sample thickness or, in the case of the olivine + albitic melt samples, smaller than the sample thickness. The compaction length of the olivine +

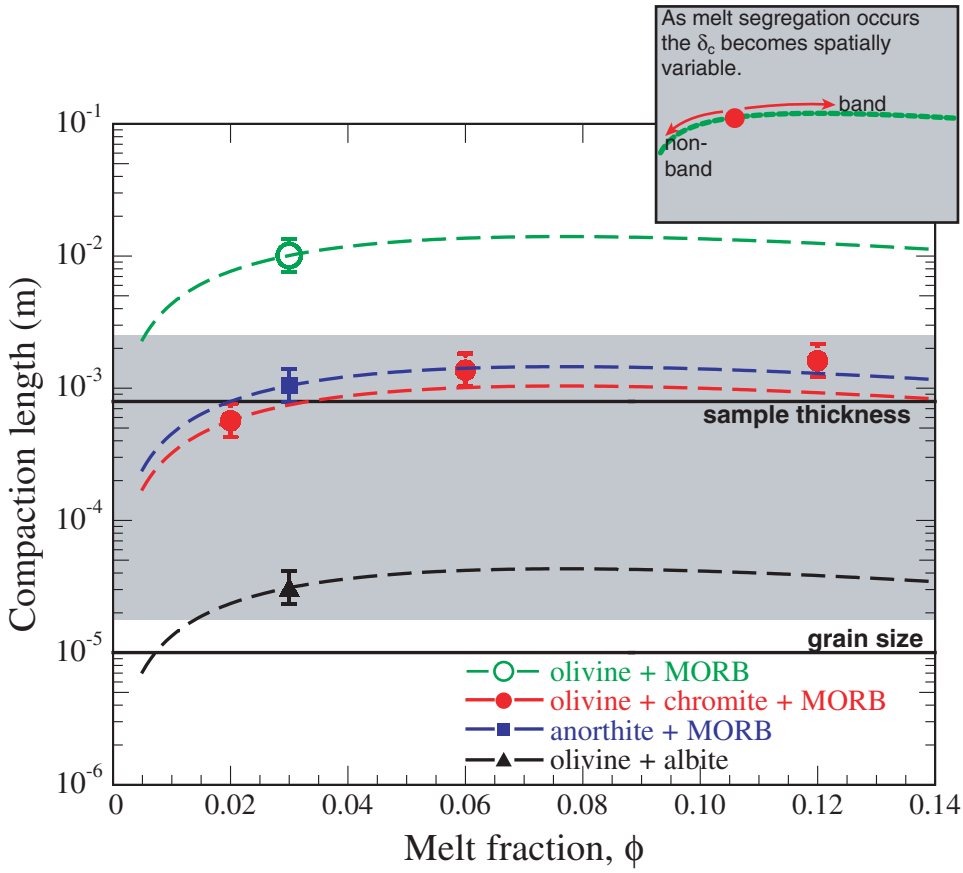

Figure 7. Compaction length as a function of melt fraction for all of the experiments described in this study. The solid symbols are calculated values of the initial compaction lengths before deformation using values reported in Table 1. The error bars are calculated assuming that the permeability carries an uncertainty of 25%. The dashed lines were calculated from the dependence of η and k on ϕ. In the experiments in which melt segregation occurs, the compaction length increases slightly inside the bands where ϕ is large but decreases rapidly between bands where ϕ is small, as indicated by the dashed lines and the inset. For reference relative to the compaction length, the upper horizontal line marks the average sample thickness and the lower marks the approximate grain size. Band formation occurred in all samples with compaction lengths falling in the field highlighted in gray.

MORB samples plots well above the sample thickness. This plot suggests that, if the sample thickness were larger, then the olivine + MORB system would form bands. In the simple-shear setup used in this study, such large sample thicknesses are not possible; however, in the recently developed torsion apparatus [*Paterson and Olgaard*, 2000], much larger samples may be deformed to much larger strains. Therefore, in the future it will be possible to test our hypothesis on the olivine + MORB system. Band formation should occur in regions of the partially molten mantle that are wider than their respective compaction lengths, which is likely to be true in most asthenospheric settings, such as subduction wedges, plumes, and mid-ocean ridges.

[31] Second, δ_c influences band morphology (i.e., spacing). In Figure 8, we plot band spacing, δ_b, as a function of δ_c, for six samples deformed to strains of $\gamma = 3.5$ and one sample (olivine + albitic melt) deformed to $\gamma = 5$. A strong linear correlation is apparent, with a slope of 0.2. (The data could be fit to an exponential curve, but with such limited data, we choose the simplest relation.) Of the numerous variables at hand (σ, k, ε, $\dot{\varepsilon}$), ε is nearly constant for the samples in this comparison, and the other three parameters are contained in the definition of the compaction length. For this reason, we believe this plot captures some of the essential physics of this problem. To compare the morphologies of melt segregation in different systems, it does not suffice

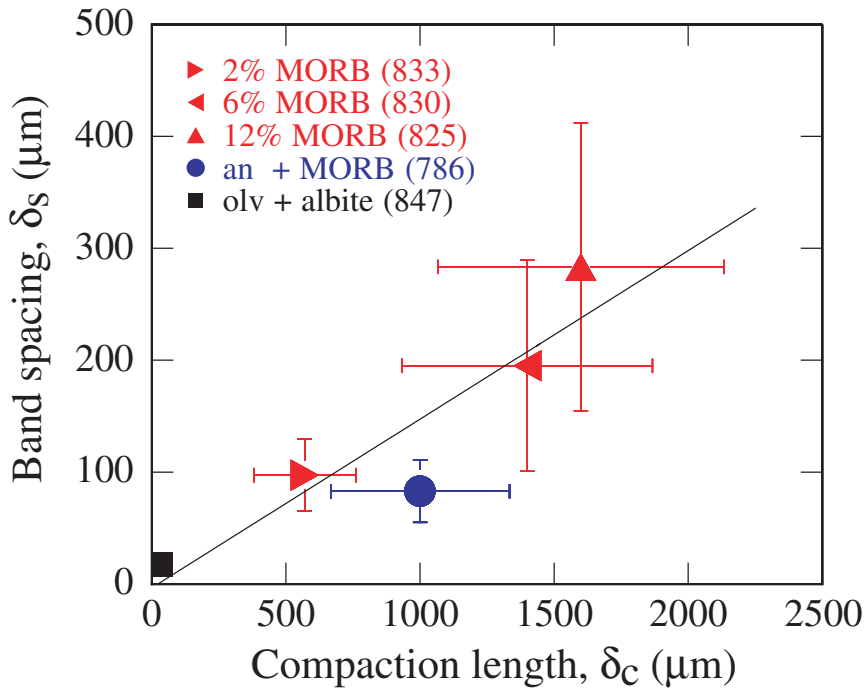

Figure 8. Band spacing as a function of compaction length. The triangular symbols are the olivine + chromite + MORB samples, with melt volumes listed in the legend. The vertical error bars are the standard deviations in the data. Error increases with band spacing because there are fewer bands per sample as the spacing increases, and thus less data. The horizontal error is the same as in Figure 7, assuming an error bar of 25% in permeability. The horizontal error increases with increasing permeability. The linear best fit has a slope of 0.15.

to compare only the driving force for segregation. The spacing is also controlled by the transport properties, described here by the permeability and the melt viscosity (though other processes, namely dissolution/precipitation may contribute to the transport of melt, as discussed in section 5.5).

[32] We estimate that the spacing between the largest bands is $\delta_b = \delta_c/5$, based on the slope of the fitted line in Figure 8, for samples deformed to similar strains. However, this estimate may only hold for the small range of compaction lengths tested in these experiments. At much longer δ_c, surface tension may have diminished importance. At smaller scales, δ_c approaches the grain scale and loses its meaning as the continuum approximation breaks down. If δ_c is too close to the grain size, then the pressure gradients caused by heterogeneities in stress at the grain scale may dominate over longer wavelength pressure gradients due to deformation. A band spacing of $\delta_c/5$ is very close to the grain size in these samples ($\delta_c/5 = 6 \times 10^{-6}$, $d = 7 \times 10^{-6}$), which means that the pressure gradients due to deformation act on the same length scales as those caused by grain-melt pocket interactions. The similarity in these length scales may explain the more irregular nature of the melt bands in the olivine + albitic melt samples compared to those in the olivine + chromite + MORB and the anorthite + MORB samples.

[33] Small melt-rich regions often form on the "leeward" side of the peaks in the piston face as the sample material is sheared, due to a low pressure region that develops as the material shears past the groove. To test the influence of the grooves in band formation, we deformed a sample of olivine + chromite + 6 vol% MORB with olivine pistons without grooves; this sample also developed bands, as shown in Figure 4. We conclude that the initiation of instabilities may be accelerated by the presence of the grooves in the piston walls, but neither the presence, nor the spacing, nor the orientation of the bands is determined by the existence of the grooves. This statement is supported by the observation that the band

morphology (spacing and thickness) in the olivine + chromite + MORB samples varies with initial melt fraction, even though the groove spacing is constant.

[34] In the following sections, we expand on 1) the microstructural-mechanical aspects of the two conclusions drawn above and 2) their implications for natural systems.

5.2. Compaction Length and the Mechanics of Melt Segregation

[35] Our experiments demonstrate that segregations with wavelengths longer than the grain scale but a fraction of the compaction length can form and persist during deformation. *Stevenson* [1989] predicted that stress could cause amplification of small perturbations in melt fraction into regions of larger-scale melt segregation, over distances smaller than the compaction length. Because of the dependence of viscosity on melt fraction, regions with slightly higher melt fractions are weaker than melt-poor regions. If strain rate is constant throughout the sample, the mean pressure will be lower in melt-rich regions than in melt-poor regions, driving melt into the weaker regions, causing them to weaken further, and so on. Analysis of Stevenson's melt segregation instability indicates that no preferred wavelength of melt segregations develops, but the wavelength will be some fraction of the compaction length [*Stevenson*, 1989; *Richardson*, 1998]. *Hall and Parmentier* [2000] suggest that the smallest wavelength instability, limited at least by the grain scale, will dominate, unless there is some other feedback process to stabilize a certain wavelength, such as the strengthening of olivine with water removal upon melting and melt extraction. In a recent formulation of compaction theory with damage mechanics [*Bercovici et al.*, 2001a, 2001b], stress accelerates self-separation of phases by adding energy to the interfaces of two fluids. In a 1-D simple shear flow, the weaker fluid separates into a layer and leads to strain localization [*Bercovici et al.*, 2001b]. While this description is similar to the behavior in our experiments, it is difficult to assess whether the physics of damage are active in the systems studied here, in which surface tension tends to hold melt in triple junctions, resisting self-separation.

[36] Although the kinematic boundary conditions are very different (pure shear vs. nearly simple shear), we believe that the dynamics of band-formation involves, to some degree, the dynamics described by Stevenson. Whether the segregations in our experiments are "instabilities" (in that they will continue to segregate until all the melt is removed from the nonband regions) or they have reached a steady state (by a shear strain of 3–3.5) is an open question. Clearly, between strains of 1 and 3, they are still developing. The increase in band spacing and melt content may be resisted by surface tension, which acts to retain a certain melt fraction in the nonband regions [e.g., *Stevenson*, 1986; *Riley and Kohlstedt*, 1991; *Wark and Watson*, 2000]. Surface tension in a two-phase system without grain boundaries (or a system in which the melt tends not to make connected networks of triple junctions [e.g., *von Bargen and Waff*, 1986]) tends instead to cause phases to separate to minimize surface area, and stress accelerates this process [*Bercovici et al.*, 2001a, 2001b]. Though it is difficult to apply their theory to the systems studied here due to the influence of grain boundaries, this self-separating behavior of a fluid phase may also play a role in the formation of melt bands. If the surface tension of wetted grain boundaries balances the forces driving melt segregation, perhaps a dynamic steady state can exist.

[37] Relative to the pure shear case discussed above, the spatial and temporal distribution of mean stresses driving melt segregation are complicated by the fact that the bands are stationary in the overall simple shear flow of the matrix. In all of the experiments discussed here, the angle between the bands and the shear plane (the piston wall) is roughly the same from one experiment to the next regardless of finite strain, between 15 and 25°, or 10–20° for anorthite. In addition, the shear stresses are of similar magnitude, between 50 and 100 MPa. This observation leads to an intriguing conclusion: because the solid is moving parallel to the piston walls (shear plane) and the melt-rich bands are nonrotating, differential movement must occur between the solid and the melt in the bands, as

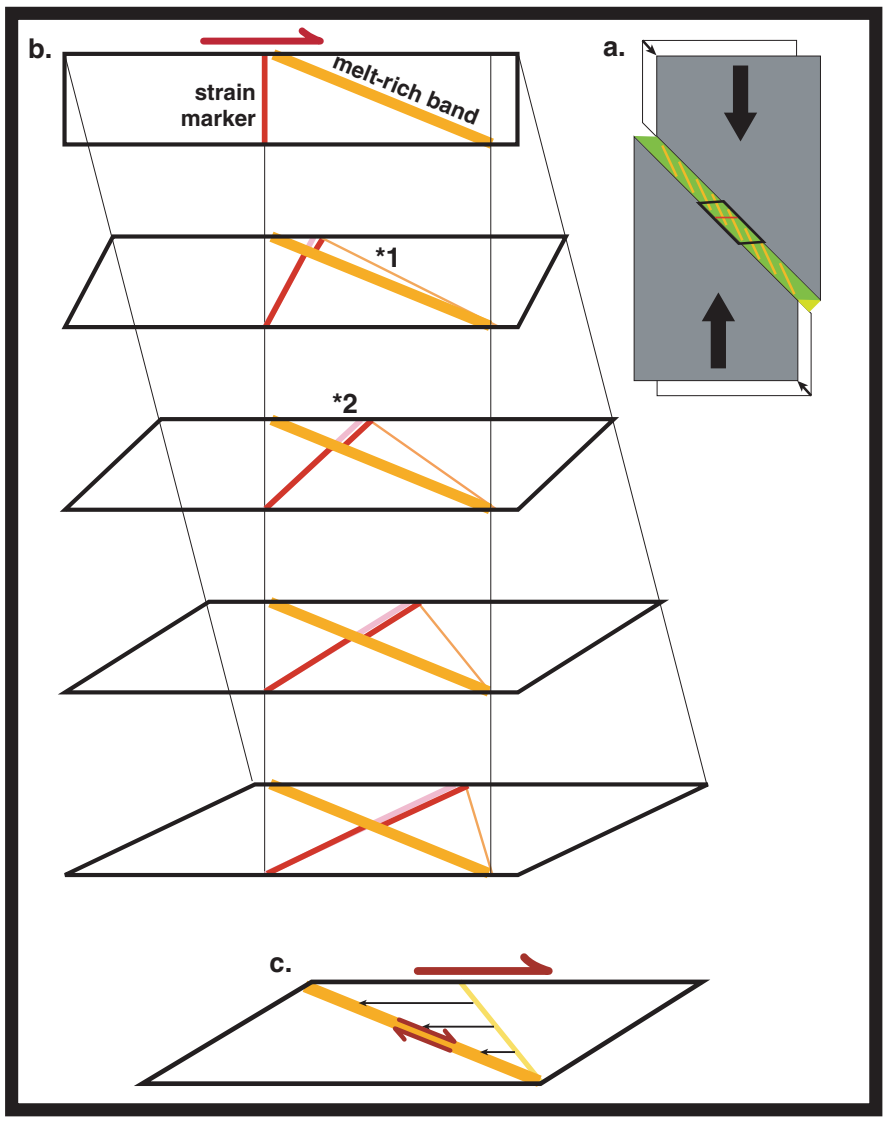

Figure 9. Schematic illustration of the kinematic constraints on a melt band at constant angle. a) The experimental reference frame illustrates how simple shear is created on the sample, and the location of the sample reference frame. b) In the sample reference frame, the lower sample wall, parallel to the shear plane, is arbitrarily fixed. The sample shears top-to-the-right, and a band forms after some time (here it is shown as existing before deformation, but that is simply to save space). *1 denotes a line that is in the position where the strain marker would be if it were fixed to the shearing solid at each time step. Similarly, *2 (pink line) marks where the strain marker would be if there were no displacement on the melt band. c) To summarize, as the melt band localizes strain, it also migrates through the solid.

illustrated in Figure 9. Therefore, the melt in a band is acting as a traveling wave with respect to the shearing solid. These waves are analogous in some ways to the gravity-driven compaction waves defined in the literature as porosity waves, melt solitons, or magmons [e.g., *Scott and Stevenson*, 1986; *Richter and McKenzie*, 1984]. However, solitons are generally noninteracting conservative waves [e.g., *Scott and Stevenson*, 1984]. If the bands interact with each other, such that small ones feed larger ones or large ones separate into smaller ones, then they are not conservative. To move through the solid, the melt band must increase melt volume at its front and decrease melt volume at its rear. The resistance of the solid to local decompaction may create the abrupt "front" or asymmetry in the melt distribution described in section 4.3. This pattern is not universal (as in

Figure 4b), perhaps indicating that the stress continuity between the band and nonband regions is very dynamic and that melt bands may adjust their angles by other means, such as the enhanced growth of low angle bands at the expense of high angle ones.

[38] Furthermore, offsets along the strain marker at points of intersection with melt-rich bands indicate that shear strain localizes on the melt bands, as illustrated in Figures 3b and 5d. Therefore, strain is partitioned into the weaker bands. This case is more complex than *Stevenson*'s [1989] analysis of 1-D pure shear in which strain rate was constant across the sample and only stress varied. This analysis is being extended to a simple shear geometry (D. J. Stevenson, personal communication, 2002; M. Spiegelman, Melt band formation by simple shear: Some analysis, submitted to *Geochemistry, Geophysics, Geosystems*, 2003). Even with strain partitioning, the mean pressure must still vary between the band and the matrix in order to drive the melt segregation. In other words, the mean stress in the band must be lower than the mean stress in the nonband regions, only if the melt is flowing down mean stress gradients in the solid. The 10–25° band angles may reflect a competition between two factors: 1) The bands would grow fastest at 45°, where the band would be normal to the least compressive stress in simple shear, similar to Stevenson's analysis, and similar to a tension gash. 2) The bands will most effectively partition strain when they are parallel to the shear plane, whereas at 45°, no partitioning would be possible. The resulting angle is a compromise. Due to strain partitioning, the measured sample viscosity eventually decreases because some part of the total strain is accommodated on the relatively weak bands. The resulting viscosity is also anisotropic. Further experiments and mechanical analysis must address questions related to the timescale of band formation, the relationship between stress and strain partitioning, and the orientation of melt-rich bands.

[39] These experiments suggest a resolution to the persistent "chicken-egg" question of whether melt segregates into shear zones or shear zones nucleate in melt-rich regions [*Kelemen and Dick*, 1995; *Rosenberg and Handy*, 2000]. Our response to this question is that it is not always an egg-chicken problem; perturbations in melt fraction and strain rate exist over a range of scales in any deforming partially molten rock, and some of these perturbations grow at the expense of others. Strain localization increases as melt segregation increases until shear zones develop.

5.3. Melt Bands and Physical Properties of Rock

[40] When stress aligns melt pockets, the permeability becomes anisotropic, as described in Appendix A and illustrated in Figure 10. As melt segregates into bands, the permeability becomes increasingly anisotropic. The permeability is highest for melt flowing in a melt band, parallel to its length (n = 3, in equation (3)), and lowest between bands, for melt flowing normal to the bands (n = 2). For the olivine + chromite + 6 vol% MORB samples, the formation of melt-rich bands (ϕ_B = 0.10–0.14) results in an anisotropy in permeability estimated at three orders of magnitude, with a maximum of $k = 5 \times 10^{-14}$ m^2 parallel to the bands and a minimum of $k = 5 \times 10^{-17}$ m^2 normal to the bands, limited by the nonband regions ($\phi_N < 0.02$). For reference, the permeability of a sample of the same grain size with a uniformly distributed melt fraction of $\phi = 0.06$ would be 1×10^{-15} m^2 (Appendix A). We use the same permeability model for the bands and nonbands, simply changing the melt fraction. However, in bands with very high melt fractions, the melt topology at the grain scale inside the bands may be more tube-like than sheet-like. This assumption would yield higher estimates of permeability than ours (n = 2 for tubes), but we use the sheet model for simplicity. The superposition of melt segregation and grain-scale anisotropy will strongly influence local permeability structures. However, their contribution to longer distance transport will depend on the interconnectedness of melt-rich regions.

[41] Melt segregation will also cause anisotropy in the viscosity of the rock. The viscosity is highly dependent on melt fraction, varying as defined in equation (2). The melt-rich bands will have a lower viscosity than the melt-poor regions, and thus

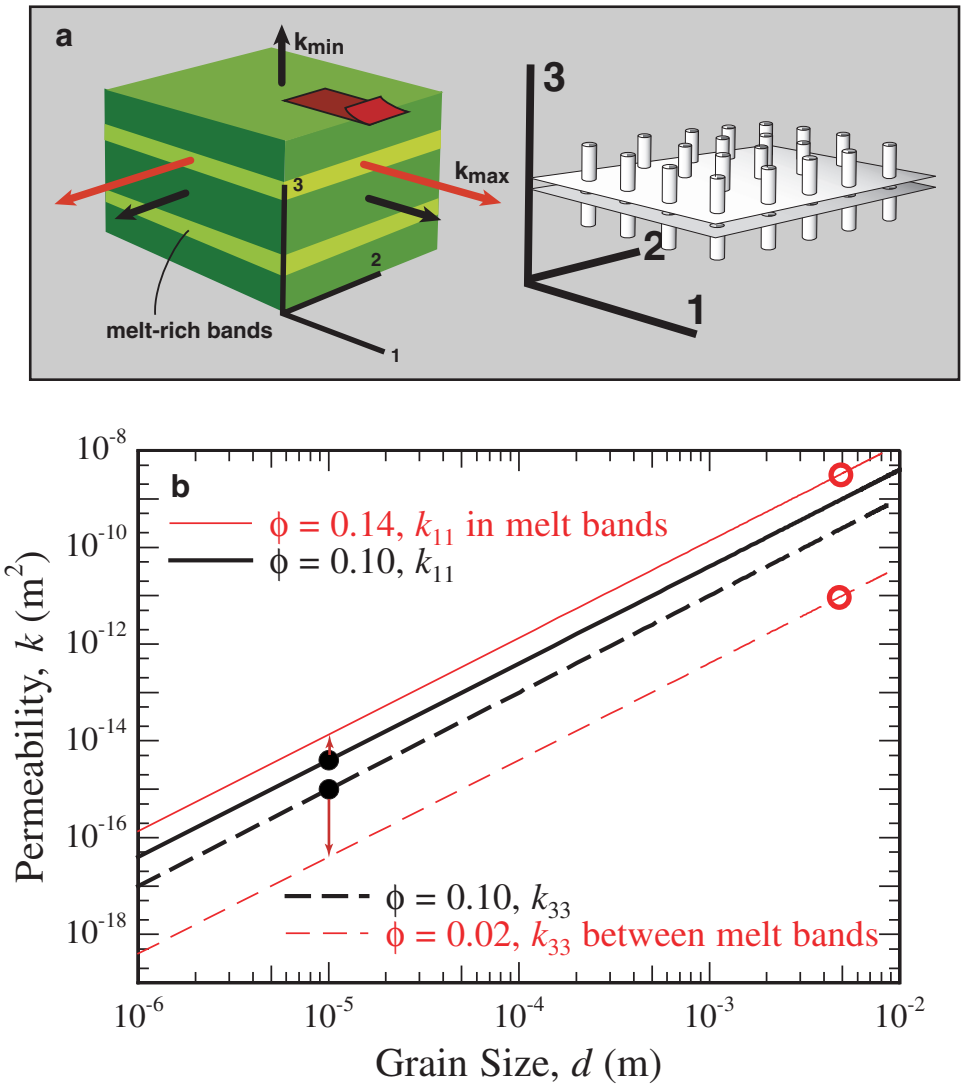

Figure 10. Permeability as a function of grain size. a) A simple "Greek temple" model of the anisotropy in permeability that develops due to the formation of bands. In the band, the tubes would be much larger diameter than in the nonband regions. b) This chart illustrates two effects: 1) The effect of melt segregation and 2) a simple scaling of the permeability. The dark circles are experimentally determined values of k for a sheared sample. The segregation of melt into bands in a sample with a homogeneous distribution of 6% melt results in large regions with 2% melt and smaller regions with 14% melt. The hollow circles are extrapolations of the experimentally determined values of k to melt contents of 2% and 14% at a mantle grain size of ~5 mm. The solid and dashed lines are extrapolations of k in grain size based on the k-d relationship given in equation (3).

strain will partition into the weaker bands. The olivine + chromite + 6% MORB sample described above would have an anisotropy in viscosity of a factor of 12 (for $\phi_B = 0.12$ in the bands, $\phi_N = 0.02$ in the nonband regions, and $\alpha = 25$ in equation (2)). Partitioning of strain into melt-rich bands may be an important mesoscale mechanism for large-scale weakening in partially molten regions of the Earth, as discussed in section 1.

[42] A layered anisotropic melt structure will also affect the elastic properties of a rock. If melt segregation occurs pervasively in space and time and the spacing between bands is smaller than the wavelength of a shear wave in the mantle (10 km), then melt-rich planes will induce shear wave splitting and a polarization anisotropy [*Kendall*, 1994; *Mainprice*, 1997]. If melt segregation occurs in a region larger than the seismic wavelength, meas-

urable shear wave splitting could occur, thus allowing a test of their presence.

5.4. Scaling to Earth Conditions

[43] To reiterate, the fact that the olivine + MORB system does not form bands is because the sample thickness is much smaller than the compaction length. In the mantle, most settings will have shear boundaries (i.e., stronger, perhaps colder, melt-free, and/or water-free regions) much farther apart than the compaction length of the partially molten region. For this reason, we believe that stress-driven melt segregation may be an important process in the Earth. To scale our experimental results to natural conditions, we assume that the segregation length scales continue to scale upward with the compaction length and then compare predicted to observed length scales of melt segregation in nature. This scaling exercise is a crude first try at a complicated problem; to scale with confidence, a much deeper understanding of the dynamics is needed, including consideration of other forces such as surface tension, which may scale differently than viscosity [e.g., *Stevenson*, 1986]. In this paper, we take the simplest approach.

[44] To scale δ_c from laboratory to natural conditions, as illustrated in Figure 5a, we must extrapolate permeability to larger grain size and viscosity to larger grain size and lower stress. Equation (4) incorporates the permeability effects illustrated in Figure 9 with the viscosity scaling discussed here. Because the viscosity for diffusion creep is independent of stress, we can scale δ_c from the value calculated for the experiments to mantle conditions using grain size alone, after *Hirth and Kohlstedt* [1995a],

$$1/\eta_{diff} = (A_{diff}/d^m)[\exp(-(E_{diff} + PV_{diff})/RT)] \quad (5)$$

where the pre-exponential term A_{diff} = 1.2 μm^3/Pa.s, the grain size d in μm, the grain size exponent m = 3, the activation energy E_{diff} = 315 kJ/mol, the activation volume $V_{diff} = 5 \times 10^{-6}$ m^3/mol, and R is the gas constant (Z. Wang et al., Activation volume for disclocation creep in olivine, submitted to *Physics of Earth and Planetary Interiors*, 2002) (hereinafter referred to as Wang et al., submitted manuscript, 2002). Because the viscosity for dislocation creep is a function of stress, we must scale δ_c to larger grain size and to lower stress, starting with this expression for η, after *Hirth and Kohlstedt* [1995b]:

$$1/\eta_{disl} = (A_{disl}\sigma^{n-1})[\exp(-(E_{disl} + PV_{disl})/RT)] \quad (6)$$

where $A_{disl} = 2.45 \times 10^{-11}$ $Pa^{-3}s^{-1}$, n = 3.5, and E_{disl} = 504 kJ/mol, P = 300 MPa, and $V_{disl} = 2 \times 10^{-5}$ m^3/mol (Wang et al., submitted manuscript, 2002). In Figure 11, the compaction lengths with diffusion and dislocation creep are juxtaposed, illustrating that the dislocation creep viscosity increases a great deal when the stress is scaled downward to stresses more representative of the asthenosphere. For a grain size of about 1 mm, the lower end of natural observed grain sizes in rocks preserving high-temperature deformation microstructures [*Ave Lallement et al.*, 1980], the δ_c-d line for the dislocation creep regime at σ = 1 MPa crosses under the δ_c-d line for the diffusion creep regime. The fact that viscosity for dislocation creep is lower than viscosity for diffusion creep at these conditions correlates well with the grain sizes and crystallographic preferred orientations observed in ophiolites, which implies that dislocation creep is an important mechanism in the high-temperature peridotites [e.g., *Nicolas*, 1989; *Ceuleneer and Rabinowicz*, 1992; *Dijkstra et al.*, 2002].

[45] To estimate band spacing from initial compaction length, we assume that the maximum band spacing is $\delta_c/5$, extending the extrapolation shown in Figure 8. The band spacing is a fraction of the initial compaction length because the compaction length in the nonband regions decreases quickly with decreasing melt fraction, as illustrated in Figure 7, reducing the distance melt can travel. If this estimate holds with scaling in stress and grain size, we predict that the band spacing will fall below the line scaling compaction length (to $\delta_c/5$) at 1 MPa in dislocation creep shown in Figure 11, yielding values to compare with the spacing between melt segregation features observed in ophiolites, discussed below. The compaction length, and thus the estimated spacing, will vary only slightly as a function of melt fraction because the increase in k with increasing ϕ is offset by the decrease of η with increasing ϕ, as illustrated in

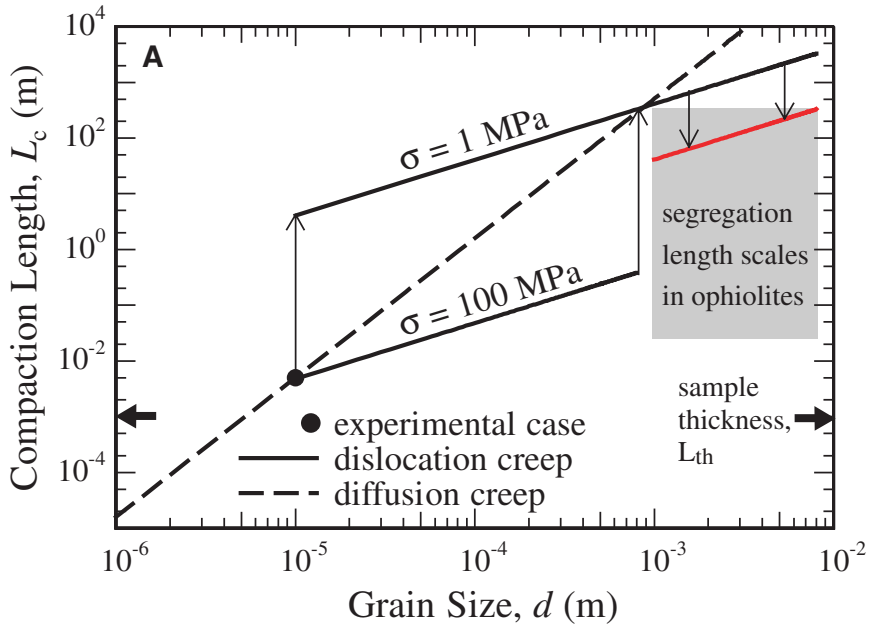

Figure 11. Compaction length as a function of grain size. The solid circle represents the value of the initial compaction length for the olivine + MORB sample, based on measured values for η and k. The diffusion creep viscosity is independent of stress, so the compaction length may be scaled directly by grain size (shown as an example only, since this sample was deforming in the dislocation creep regime.) The dislocation creep flow law is a function of stress, so we scale first to lower stress (the vertical arrows) and then to increasing grain size. From the compaction length values at mantle grain sizes, we drop the red line by one order of magnitude, to the estimated spacing between bands, which lies in the gray field describing length scales of melt segregation-related features in ophiolites. The scaling approach is discussed in more detail in the text.

Figure 3. However, viscosity for dislocation creep decreases with increasing stress. Predicted compaction lengths for the uppermost mantle at a stress level of 1 MPa are on the order of δ_c = 300–3000 m, such that stress-driven melt segregation bands should be separated at most by 50–500 m (δ_c/5). A stress of 10 MPa would cause maximum band spacings on the order of 10–100 m for mantle grain sizes of 1–10 mm. This stress level is estimated for the uppermost mantle in the Oman ophiolite by *Dijkstra et al.* [2002].

5.5. Do We See Deformation-Driven Melt Segregation in Nature (Especially in Oman)?

[46] In this paper, we focus on the melt migration processes involving two-phase flow, that is, porous flow of the fluid and plastic flow of the solid matrix, as opposed to flow through fractures. In the Oman and other ophiolites, the rock record describes a very complex history of magmatism and deformation in the uppermost 5–10 km of the mantle beneath a spreading center [e.g., *Nicolas*, 1989; *Ceuleneer and Rabinowicz*, 1992; *Ceuleneer et al.*, 1996; *Jousselin et al.*, 1998; *Koga et al.*, 2001]. We will discuss two distinct sorts of features indicative of melt–rock interaction at high temperature (1200–1250°C), tabular dunites in harzburgite and plagioclase bands in the dunitic Moho transition zone. We suggest that these features may also represent, in addition to magmatic processes, interactions between melt migration and deformation.

5.5.1. Tabular Dunites in Harzburgite

[47] Tabular dunites form as basalt rises toward the surface faster than it can equilibrate with its host, becoming increasingly undersaturated in clinopyroxene [e.g., *Kelemen et al.*, 1995]. These basalts dissolve pyroxene in the host rock and precipitate olivine, as melt fraction increases, producing dunites which demarcate the path traveled by the melt. If the melt fraction in a dunite is relatively constant, then the dunite represents the whole porous flow channel and/or dunites represent reaction rims

around periodically open conduits, in which case the flux is more difficult to estimate [e.g., *Nicolas*, 1986; *Suhr*, 1999]. Regardless of the process by which melt is moving through them, they represent an important component of the melt extraction process. The problem we can address most directly in light of these experiments is the mechanism by which the melt initially segregates from a region in which melt production is spatially homogeneous.

[48] A well-explored hypothesis connecting dunite formation and melt segregation involves the "reaction infiltration instability" in which a fluid (basalt) undersaturated in one phase (clinopyroxene) migrates into a matrix which contains that phase and another phase in which the fluid is oversaturated (olivine) [e.g., *Daines and Kohlstedt*, 1993; *Aharonov et al.*, 1995]. In the mantle, as basalt dissolves pyroxene, the melt fraction increases, which increases the permeability. This increase in permeability increases the flux, and thus reduces the time available for melt-rock interaction, extending the solubility gradient. This process tends to produce runaway instabilities which take the form of channels organized into a coalescing network [e.g., *Spiegelman et al.*, 2001]. One compelling connection between theory and observation is the prediction and observation of self-similarity in dunite length scales.

[49] In the mantle sections of the Oman and Ingalls ophiolite, dunites have a power law dependence of abundance on width [*Kelemen et al.*, 2000; *Braun and Kelemen*, 2002]. In the Ingalls ophiolite, tabular dunite bodies have widths ranging from approximately 0.1 to 2 m [*Kelemen et al.*, 2000], with spacings on similar length scales. In the Oman ophiolite, widths range from 5 mm to 100 m [*Kelemen et al.*, 2000; *Braun and Kelemen*, 2002]. In the Bay of Islands ophiolite, Newfoundland, large tabular dunites, 10–50 m wide (maximum 100 m), are spaced 300–600 m apart (G. Suhr, unpublished data, 2001).

[50] We believe that the process of stress-driven melt segregation may be important in the initial segregation of melt into channels. The maximum length scales of melt segregation predicted by scaling the compaction length agree well with the thicknesses and spacings of the larger tabular dunites in Oman and in Newfoundland, suggesting that reaction-driven and stress-driven melt segregation may be interacting processes. In the deeper levels of the melting column, where channelization is occurring and networks are forming, stress-driven segregation may either nucleate on and accelerate reaction-driven instabilities or create initial pathways for the inception of dissolution. Further up in the melting region, as both melt segregation and strain rates increase, the partitioning of strain into melt-rich zones may have a growing influence on mantle flow, as suggested in the early studies of corner flow with melt-weakening discussed in the introduction.

5.5.2. Plagioclase Bands in the Dunitic Mantle Transition Zone

[51] The "massive", as opposed to "tabular", dunites observed in the Oman ophiolite form by melt ponding beneath the Moho, dissolving pyroxene from harzburgite and crystallizing olivine [*Boudier and Nicolas*, 1995, *Koga et al.*, 2001]. Within these large dunites, up to 500 m thick, local plagioclase-rich lenses or bands are observed in which plagioclase has crystallized between olivine grains, referred to as "impregnated dunites" [e.g., *Ceuleneer and Rabinowicz*, 1992; *Nicolas and Boudier*, 1995]. *Koga et al.* [2001] demonstrate with major and rare earth element chemistry that these plagioclase crystals are not trapped melt, but are the products of fractional crystallization in an open system. The plagioclase may represent the partial crystallization of migrating basalts as the melts cross isotherms and become saturated in plagioclase (and cpx) [*Koga et al.*, 2001; *Kelemen and Aharonov*, 1998]. When crystallization occurs, local permeability may decrease dramatically [*Kelemen and Aharonov*, 1998]. The point is that neither the crystal forms nor the volume of plagioclase represent melt fraction at an instant. However, the distribution of plagioclase-rich lenses and layers in the Moho transition zone is very heterogeneous. When these features occur as parallel streaks or discontinuous layers, as in the Lanzo massif [*Boudier*, 1978] and in Oman (Figure 12) [*Ceuleneer and Rabinowicz*, 1992], they may rep-

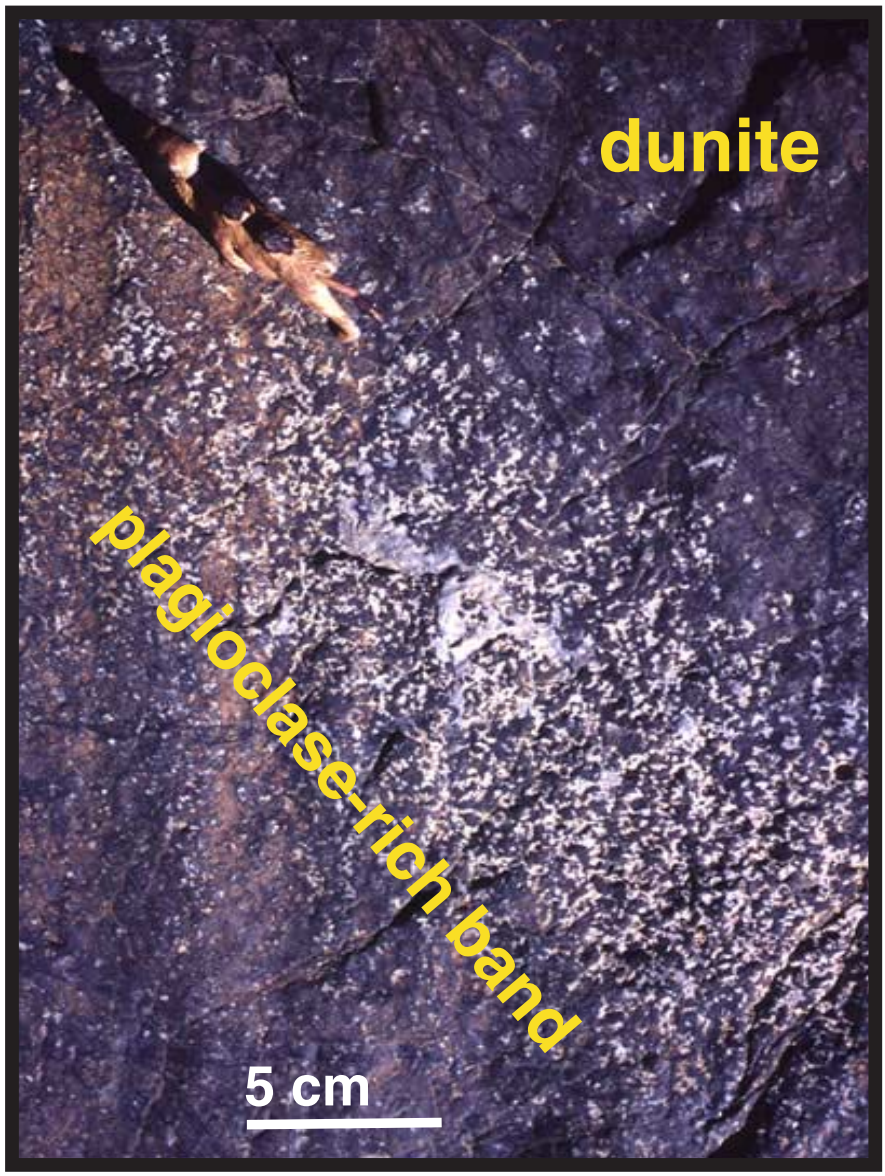

Figure 12. Plagioclase-rich band in massive dunite in the Oman ophiolite. The plagioclase crystallized from a basaltic melt flowing through a permeable dunite (please see discussion in section 5.5.2). This band lies between two parallel, 20-cm wide bands spaced about 1 m apart (original observations, B.K.H., 2001). The localized crystallization of plagioclase occurred in an open system and does not represent a trapped, frozen melt. However, the parallel layers may represent traces of segregated melt flow at some (late?) stage in the life of the magmatic system, and thus may represent a process similar to that observed in experiment. The plastic camel, ~5-cm long, is facing toward the Moho. Mahram outcrop, Semail Massif, Oman.

resent traces of melt segregation processes similar to those in our experiments.

[52] We suggest that these layers may be traces, but not frozen instances, of segregated flow of melt through the transition zone. For example, the observed width of the plagioclase band may represent crystallization only on the margin of a conduit, not the width of the conduit. Though it is difficult to determine the genesis of plagioclase-rich bands, these layers may be distinct evidence for segregated flow caused by deformation, since the reaction infiltration instability could not operate in the dunite transition zone that is already free of

soluble clinopyroxene. We cannot determine an instantaneous melt distribution from an observed distribution of plagioclase and cpx, but a heterogeneous distribution of crystals implies a heterogeneous distribution of migrating melt. The plagioclase band in Figure 12 is 0.2 m wide and is separated from two similar bands by 1 m. Another example of plagioclase banding occurs in lherzolites of the Lanzo peridotite massif, with segregation length scales on the order of 0.1–1 m [*Boudier*, 1978]. The bands in Lanzo are smaller and more closely spaced than those in Oman. Both observed spacings are smaller than the 10–500 m upper limit we predict based on the simple compaction length extrapolation, which may reflect lower temperature and/or higher stress conditions than used in the scaling exercise illustrated in Figure 10 and described in section 5.4.

5.6. More Speculation

[53] Extrapolation to deforming, melting regions of the mantle involves (at least) higher pressures, compositional heterogeneities, larger grain sizes, lower stresses, and different boundary conditions. Scaling with compaction length offers a very simplistic first step, but avoids many difficult questions. In this section, we raise several questions that may factor into natural, but not experimental, systems, including possible interactions with compositional heterogeneities, roles of visco-elasticity, and large-scale self-organization of channels and networks.

[54] Stress-driven melt segregation may strongly interact with compositional heterogeneities in the upwelling, melting mantle. For example, pyroxenite bodies will begin to melt deeper than lherzolite beneath a ridge or a hot spot [*Hirschmann and Stolper*, 1996; *Phipps Morgan and Morgan*, 1999]. These pyroxenites provide a local source of melt and thus viscosity perturbations that could nucleate deformation-driven melt segregation. In this case, the melt is localized or partially presegregated, and deformation would therefore create an initial pathway for melt transport.

[55] Another line of questions concerns what happens to isolated bands or layers of melt once they form (if they are not always in networks of connected channels). If isolated, they may rise as waves driven by their own buoyancy. As discussed above, they may nucleate dissolution instabilities. Anywhere along the transport path, if the melt velocity is high enough and local changes in melt fraction cause dilational strains over timescales shorter than the local visco-elastic relaxation times, elastic properties of the rock may control the local melt migration mechanism [e.g., *Connoly and Podladchikov*, 1998]; this transition to elastic behavior may lead to the formation of nondilatent, melt-filled shear fractures (J. Phipps Morgan and B. Holtzman, Vug waves: A mechanism for coupled rock deformation and fluid migration, manuscript in preparation, 2003).

[56] At larger scales, how might melt segregation bands interact as a self-organizing system? Clearly, the networks visible in the olivine + chromite + MORB samples in Figure 4 are strongly influenced by the geometry of the experiment, making extrapolation to natural settings more difficult. Solving this problem will involve a detailed understanding of the appropriate governing physical processes, which will likely require solving the nonlinear equations of compaction with a strong dependence of viscosity on melt fraction. The boundary conditions of the geodynamic setting (such as the spreading rate at the ridge and the geometry of the lithospheric walls or the slab angle and degree of coupling in a subduction zone) as well as rates of melt productivity and degrees of melt-solid disequilibria may strongly influence the spatial and temporal distribution of melt bands, their orientations, and their connectivity. In nature, the orientations of principal stresses will be much more complicated than in our experiments, as will the compositional, thermal, and thus rheological variations in the system, all of which will influence the dynamics of melt segregation and strain localization.

6. Conclusions

[57] Stress-driven melt segregation is important for understanding melt segregation and transport in lower crust and upper mantle rocks. A more complete scaling from laboratory to natural sys-

tems will require a much better understanding of the dynamics occurring in the experiments. Application to natural settings must include effects of anisotropy in permeability and viscosity as well as their influences on different geodynamic environments, characterized by different stress fields. If melt segregation occurs pervasively in space and time with spacings less than the wavelength of a shear wave in the mantle (~10 km), then melt-rich planes will induce shear wave splitting and a polarization anisotropy. Melt-enriched planar structures with orientations controlled by the stress field characteristic of the geodynamic environment (mid-ocean ridges, subduction zones, rising plumes) will influence mantle dynamics through feedbacks between deformation, stress fields, and evolving mechanisms of solid and melt transport.

Appendix A

[58] The permeability of the olivine + MORB system was quantified in the following manner [*Scott*, 2000]: From a sample with $\phi = 0.10$, reflected light images of polished serial sections separated by 1 μm were digitally photographed, and image analysis was used to visualize the melt fraction. The digital serial images were stacked, then interpolated between sections and voxelized to create volumes containing a 3-D structure of melt. The melt-rich regions visible in the digital volumes (http://olivine.geo.umn.edu) can be approximated by sheets formed by the planes of oriented melt pockets spanning the length of several grains; these sheets are connected by more tube-like grain-boundary triple-junctions.

[59] A lattice-Boltzmann simulation of flow through the voxel-volume was performed by Dr. J. Frederich (Sandia National Laboratories) to determine the permeability. For one sample, the maximum permeability measured parallel to the shear plane is 4×10^{-15} m^2, and the minimum measured perpendicular to the shear plane is 1×10^{-15} m^2.

[60] To extrapolate these values to other samples, with different grain sizes and melt fractions, we use equation (3). Based on the melt topology observations, we used $n = 3$ for the maximum and intermediate permeability directions that form the plane, and $n = 2$ for the tubes normal to the plane, to estimate the principle directions of a permeability tensor. Pinning the permeability curves to the measured values yields a geometric factor $b = 1000$, for $n = 2$, and $b = 25$, for $n = 3$. Since the compaction process that forms melt bands requires melt to move normal to the sheets and melt bands, the minimum ($n = 2$) permeability definition was used; n = 3 is used for the flow parallel to sheets.

[61] The permeability of the olivine + chromite + MORB samples is significantly lower than that of olivine + MORB, because chromite grains sit in melt-filled 3- or 4-grain junctions, reducing the throat size of the melt paths. We estimated the effect of chromite grains on the permeability by solving for the reduction in throat area when a sphere is placed in a triple junction and calculating the radius of a circle with an area equal to the cross-sectional area of the three tubes around the chromite sphere (reduced area by about 1/3). Then, using equation (5.10.8) of *Bear* [1988], describing the effect of a constriction in a melt pathway originally derived by *Scheidegger* [1974], we assumed that 1/10 of each tube connecting a sheet has this constricted area. This approach yields a reduction of permeability by a factor of 0.1, hence, we used a value of $b = 10000$ when $n = 2$.

Acknowledgments

[62] This paper grew and improved in conversations with J. Phipps Morgan, J. Tullis, R. Cooper, S. Majumder, M. Daines, G. Suhr, M. Hirschmann, M. Spiegelman, and many others. B. Holtzman also wishes to thank the members of the Laboratoire de Tectonophysique, Université de Montpellier II, France, for generous welcome, well-fed discussions, and excursions in Oman and Lanzo. This paper benefited greatly from critical reviews by Brian Evans, David Stevenson, and Peter Kelemen. The research was funded by NSF grants OCE-0002463, EAR-0126277, and EAR-9906986, and NASA grant NAG5-10509, and a Fulbright Fellowship for study in France to B. Holtzman.

References

Aharonov, E., J. A. Whitehead, P. B. Kelemen, and M. Spiegelman, Channeling instability of upwelling melt in the mantle, *J. Geophys. Res.*, *100*(10), 20,433–20,450, 1995.

Ave Lallement, H., J.-C. Mercier, N. Carter, and J. V. Ross, Rheology of the upper mantle: Inferences from peridotite xenoliths, *Tectonophysics*, *70*, 85–113, 1980.

Bear, J., *Dynamics of Fluids in Porous Media*, Dover, Mineola, N. Y., 1988.

Bercovici, D., Y. Ricard, and G. Schubert, A two-phase model for compaction and damage, 1, General theory, *J. Geophys. Res.*, *106*, 8887–8906, 2001a.

Bercovici, D., Y. Ricard, and G. Schubert, A two-phase model for compaction and damage, 3, Applications to shear localization and plate boundary formation, *J. Geophys. Res.*, *106*, 8925–8940, 2001b.

Boudier, F., Structure and petrology of the Lanzo peridotite massif (Piedmont Alps), *Geol. Soc. Am. Bull.*, *89*, 1574–1591, 1978.

Boudier, F., and A. Nicolas, Nature of the Moho Transition Zone in the Oman ophiolite, *J. Petrol.*, *36*, 777–796, 1995.

Braun, M. G., and P. B. Kelemen, Dunite distribution in the Oman Ophiolite: Implications for melt flux through porous dunite conduits, *Geochem. Geophys. Geosyst.*, *3*(11), 8603, doi:10.1029/2001GC000289, 2002.

Brown, M., and G. Solar, Shear-zone systems and melts: Feedback relations and self-organization in orogenic belts, *J. Struct. Geol.*, *20*(2/3), 211–227, 1998.

Buck, R., and W. Su, Focused mantle upwelling below mid-ocean ridges due to feedback between viscosity and melting, *Geophys. Res. Lett.*, *16*, 641–644, 1989.

Burg, J.-P., Syn-migmatization way-up criteria, *J. Struct. Geol.*, *13*(6), 617–623, 1991.

Ceuleneer, G., and M. Rabinowicz, Mantle flow and melt migration beneath oceanic ridges: Models derived from observations in ophiolites, in *Mantle Flow and Melt Generation at Mid-ocean Ridges*, *Geophys. Monogr. Ser.*, vol. 71, edited by J. Phipps Morgan, D. K. Blackman, and J. M. Sinton, pp. 123–154, AGU, Washington, D. C., 1992.

Ceuleneer, G., M. Monnereau, and I. Amri, Thermal structure of a fossil mantle diapir inferred from the distribution of mafic cumulates, *Nature*, *379*, 149–153, 1996.

Connoly, J., and Y. Podladchikov, Compaction-driven flow in visco-elastic rock, *Geodyn. Acta*, *11*, 55–84, 1998.

Cooper, R., Differential stress induced melt migration: An experimental approach, *J. Geophys. Res.*, *95*(B5), 6979–6992, 1990.

Cordery, M. J., and J. Phipps Morgan, Melting and mantle flow beneath a mid-ocean spreading center, *Earth Planet. Sci. Lett.*, *111*(2–4), 493–516, 1992.

Daines, M. J., and D. L. Kohlstedt, A laboratory study of melt migration, *Philos. Trans. R. Soc. London*, *342*, 43–52, 1993.

Dell'Angelo, L. N., and J. Tullis, Experimental deformation of partially melted granitic aggregates, *J. Metamorph. Geol.*, *6*, 495–515, 1988.

Dijkstra, A. H., M. R. Drury, and R. M. Frijhoff, Microstructures and lattice fabrics in the Hilti mantle section (Oman Ophiolite): Evidence for shear localization and melt weakening in the crust-mantle transition zone?, *J. Geophys. Res.*, *107*(B11), 2270, doi:10.1029/2001JB000458, 2002.

Dimanov, A., G. Dresen, and R. Wirth, High-temperature creep of partially molten plagioclase aggregates, *J. Geophys. Res.*, *103*(B5), 9651–9664, 1998.

Ghiorso, M., and R. Sack, Chemical mass transfer in magmatic processes, IV, A revised and internally consistent thermodynamic model for the interpolation and extrapolation of liquid-solid equilibria in magmatic systems at elevated temperatures and pressures, *Contrib. Mineral. Petrol.*, *119*, 1971995.

Hall, C. E., and E. M. Parmentier, Spontaneous melt localization in a deforming solid with viscosity variations due to water weakening, *Geophys. Res. Lett.*, *27*(1), 9–12, 2000.

Hirschmann, M. M., and E. M. Stolper, A possible role for garnet pyroxenite in the origin of the "garnet signature" in MORB, *Contrib. Mineral. Petrol.*, *124*(2), 185–208, 1996.

Hirth, G., and D. L. Kohlstedt, Experimental constraints on the dynamics of the partially molten upper mantle: Deformation in the diffusion creep regime, *J. Geophys. Res.*, *100*, 1981–2001, 1995a.

Hirth, G., and D. L. Kohlstedt, Experimental constraints on the dynamics of the partially molten upper mantle, 2, Deformation in the dislocation creep regime, *J. Geophys. Res.*, *100*, 15,441–15,449, 1995b.

Hollister, L., and M. L. Crawford, Melt-enhanced deformation: A major tectonic process, *Geology*, *14*, 55–59, 1986.

Holtzman, B., The interactions of deformation and melt migration in the Earth, Ph.D. thesis Univ. of Minn., Minneapolis, 2003.

Ildefonse, B., S. Billiau, and A. Nicolas, A detailed study of mantle flow away from diapirs in the Oman ophiolite, in *Mantle Crust and Lower Crust Exposed in Oceanic Ridges and in Ophiolites*, edited by R. L. M. Vissers and A. Nicolas, pp. 163–177, Kluwer Acad., Norwell, Mass., 1995.

Jousselin, D., A. Nicolas, and F. Boudier, Detailed mapping of a mantle diapir below a paleo-spreading center in the Oman ophiolite, *J. Geophys. Res.*, *103*(B8), 18,153–18,170, 1998.

Kelemen, P., and E. Aharonov, Periodic formation of magma fractures and generation of layered gabbros in the lower crust beneath oceanic spreading centers, in *Faulting and Magmatism at Mid-ocean Ridges*, *Geophys. Monogr. Ser.*, vol. 106, edited by W. R. Buck et al., pp. 267–289, AGU, Washington D. C., 1998.

Kelemen, P. B., and H. J. B. Dick, Focused melt flow and localized deformation in the upper mantle: Juxtaposition of replacive dunite and ductile shear zones in the Josephine Peridotite, SW Oregon, *J. Geophys. Res.*, *100*(1), 423–438, 1995.

Kelemen, P. B., N. Shimizu, and V. J. M. Salters, Extraction of mid-ocean-ridge basalt from the upwelling mantle by focused flow of melt in dunite channels, *Nature*, *375*(6534), 747–753, 1995.

Kelemen, P. B., G. Hirth, N. Shimizu, M. Spiegelman, and H. J. B. Dick, A review of melt migration processes in the adiabatically upwelling mantle beneath oceanic spreading ridges, *Philos. Trans. R. Soc. London*, *355*, 283–318, 1997.

Kelemen, P. B., M. Braun, and G. Hirth, Spatial distribution of melt conduits in the mantle beneath oceanic spreading ridges: Observations from the Ingalls and Oman ophiolites, *Geochem. Geophys. Geosyst.*, *1*, doi:10.1029/1999GC000012, 2000.

Kendall, J. M., Teleseismic arrivals at a mid-ocean ridge: Effects of mantle melt and anisotropy, *Geophys. Res. Lett.*, *21*, 301–304, 1994.

Koga, K. T., P. B. Kelemen, and N. Shimuzu, Petrogenesis of the crust-mantle transition zone and the origin of lower crustal wehrlite in the Oman ophiolite, *Geochem. Geophys. Geosyst.*, *2*, doi:10.1029/2000GC000132, 2001.

Kohlstedt, D. L., and M. E. Zimmerman, Rheology of partially molten mantle rocks, *Annu. Rev. Earth Planet. Sci.*, *24*, 41–62, 1996.

Lamoureux, G., B. Ildefonse, and D. Mainprice, Modelling the seismic properties of fast-spreading ridge crustal Low-Velocity Zones: Insights from Oman gabbro textures, *Tectonophysics*, *312*, 283–301, 1999.

Mainprice, D., Modelling the anisotropic properties of partially molten rocks found at mid-ocean ridges, *Tectonophysics*, *279*, 161–179, 1997.

McKenzie, D., The generation and compaction of partially molten rock, *J. Petrol.*, *25*(3), 713–765, 1984.

McKenzie, D., and M. Holness, Local deformation in compacting flows: Development of pressure shadows, *Earth Planet. Sci. Lett.*, *180*, 169–184, 2000.

Mei, S., W. Bai, T. Hiraga, and D. Kohlstedt, Influence of melt on the creep behavior of olivine-basalt aggregates under hydrous conditions, *Earth Planet. Sci. Lett.*, *201*, 491–507, 2002.

Michibayashi, K., L. Gerbert-Gaillard, and A. Nicolas, Shear sense inversion in the Hilti mantle section (Oman ophiolite) and active mantle uprising, *Mar. Geophys. Res.*, *21*, 259–268, 2000.

Nicolas, A., A melt extraction model based on structural studies in mantle peridotites, *J. Petrol.*, *27*, 999–1022, 1986.

Nicolas, A., *Structure of Ophiolites and Dynamics of Oceanic Lithosphere*, 367 pp., Kluwer Acad., Norwell, Mass., 1989.

Paterson, M., and D. Olgaard, Rock deformation tests to large shear strains in torsion, *J. Struct. Geol.*, *22*, 1341–1358, 2000.

Phipps Morgan, J., Melt migration beneath mid-ocean spreading centers, *Geophys. Res. Lett.*, *14*, 1238–1241, 1987.

Phipps Morgan, J., and W. J. Morgan, Two-stage melting and the geochemical evolution of the mantle: A recipe for mantle plum-pudding, *Earth Planet. Sci. Lett.*, *170*(3), 215–239, 1999.

Poirier, J.-P., *Creep of Crystals*, 260 pp., Cambridge Univ. Press, New York, 1985.

Rabinowicz, M., G. Ceuleneer, and A. Nicolas, Melt segregation and flow in mantle diapirs below spreading centers: Evidence from the Oman ophiolite, *J. Geophys. Res.*, *92*(B5), 3475–3486, 1987.

Renner, J., K. Viskupic, G. Hirth, and B. Evans, Melt extraction from partially molten peridotites, *Geochem. Geophys. Geosyst.*, *4*, doi:10.1029/2002GC000369, in press, 2003.

Richardson, C. N., Melt flow in a variable viscosity matrix, *Geophys. Res. Lett.*, *25*(7), 1099–1102, 1998.

Richardson, C. N., J. R. Lister, and D. McKenzie, Melt conduits in a viscous porous matrix, *J. Geophys. Res.*, *101*(9), 20,423–20,432, 1996.

Richter, F. M., and D. McKenzie, Dynamical models for melt segregation from a deformable matrix, *J. Geol.*, *92*(6), 729–740, 1984.

Riley, G. N., Jr., and D. L. Kohlstedt, Kinetics of melt migration in upper mantle-type rocks, *Earth Planet. Sci. Lett.*, *105*, 500–521, 1991.

Rosenberg, C. L., and M. R. Handy, Synthectonic melt pathways during simple shearing of a partially molten rock analogue (norcamphor-benzamide), *J. Geophys. Res.*, *105*(2), 3135–3149, 2000.

Rubin, A. M., Dike ascent in partially molten rock, *J. Geophys. Res.*, *103*(B9), 20,901–20,919, 1998.

Scheidegger, A. E., *The Physics of Flow Through Porous Media*, Univ. of Toronto Press, Toronto, Canada, 1974.

Scott, T., Lattice-Boltzmann calculation of the permeability of MORB in peridotite, M.Sc. thesis, Univ. of Minn., Minneapolis, 2000.

Scott, D. R., and D. J. Stevenson, Magma ascent by porous flow, *J. Geophys. Res.*, *91*(9), 9283–9296, 1986.

Scott, D. R., and D. J. Stevenson, A self-consistent model of melting, magma migration, and buoyancy-driven circulation beneath mid-ocean ridges, *J. Geophys. Res.*, *94*(3), 2973–2988, 1989.

Shaw, H. R., Viscosities of magmatic silicate liquids: An empirical method of prediction, *A. J. Sci.*, *272*, 870–893, 1972.

Spiegelman, M., and P. Kenyon, The requirements for chemical disequilibrium during magma migration, *Earth Planet. Sci. Lett.*, *109*, 611–620, 1992.

Spiegelman, M., and D. McKenzie, Simple 2-D models for melt extraction at mid-ocean ridges and island arcs, *Earth Planet. Sci. Lett.*, *83*, 368–377, 1987.

Spiegelman, M., P. B. Kelemen, and E. Aharonov, Causes and consequences of flow organization during melt transport: The reaction infiltration instability in compactible media, *J. Geophys. Res.*, *106*(B2), 2061–2078, 2001.

Stevenson, D. J., On the role of surface tension in the migration of melts and fluids, *Geophys. Res. Lett.*, *13*(11), 1149–1152, 1986.

Stevenson, D. J., Spontaneous small-scale melt segregation in partial melts undergoing deformation, *Geophys. Res. Lett.*, *16*(9), 1067–1070, 1989.

Suhr, G., Melt migration under oceanic ridges: Inferences from reactive transport modelling of upper mantle hosted dunites, *J. Petrol.*, *40*(4), 575–599, 1999.

Turcotte, D., and G. Schubert, *Geodynamics*, John Wiley, New York, 1982.

Urbain, G., Y. Bottinga, and P. Richet, Viscosity of liquid silica, silicates, and aluminosilicates, *Geochim. Cosmochim. Acta*, *46*, 1061–1072, 1982.

von Bargen, N., and H. S. Waff, Permeabilities, interfacial areas and curvatures of partially molten systems: Results of numerical computations of equilibrium microstructures, *J. Geophys. Res.*, *91*(B9), 9261–9276, 1986.

Wark, D., and B. Watson, Effect of grain size on the distribution and transport of deep-seated fluids and melts, *Geophys. Res. Lett.*, *27*(14), 2029–2032, 2000.

Zimmerman, M. E., S. Zhang, D. L. Kohlstedt, and S. I. Karato, Melt distribution in mantle rocks deformed in shear, *Geophys. Res. Lett.*, *26*(10), 1505–1508, 1999.